Novel Concepts for Power Electronics Control:

Introducing the Dynamic Physical Limits, the Average Natural Trajectories, and the Centric-Based Controller

by

Ignacio Galiano Zurbriggen

Ing., Universidad Nacional de Córdoba, 2010

A THESIS SUBMITTED IN PARTIAL FULFILLMENT OF
THE REQUIREMENTS FOR THE DEGREE OF

MASTER OF APPLIED SCIENCE

in

The Faculty of Graduate and Postdoctoral Studies

(Electrical & Computer Engineering)

THE UNIVERSITY OF BRITISH COLUMBIA

(Vancouver)

September 2013

Abstract

Controllers are an essential component in power conversion systems that have a significant impact on characteristic features such as performance, efficiency, size, and cost, among many others. During the last four decades, countless efforts have been made to find better controllers for power electronics systems in order to improve the converters steady state and dynamic behaviour, increase power densities and reduce losses in the system.

Small-signal based linear controllers have been the preferred alternative during decades. This technique features fixed switching frequency and low computation/sensing requirements, while the dynamic response can be improved to only a limited extent and the global stability cannot be ensured. On the other hand, excellent dynamic performances and global stability are achieved by boundary controllers, in which the switching frequency is variable and faster sensors are required.

The first part of this work presents a practical tool which allows to objectively quantize improvements made by the controllers to the performance of power converters. The theoretical optimal dynamic behaviour of buck converters is determined, analyzed, and characterized using closed-form mathematical expressions, setting a strong benchmark point for the performance evaluation.

Taking the physical limits of dynamic performance into account, and merging the advantages of linear and boundary techniques, a novel control scheme is developed for buck converters. The proposed controller is based on a large-signal model introduced here: the Average Natural Trajectories (ANTs). Enhanced dynamic performance and global stability

are achieved while low sensing and computational requirements are maintained, which makes the technique very appealing for use in high-volume production applications.

Due to the outstanding results in the basic buck converter, and in order to illustrate the application of the ideas introduced in this work for different topologies, the ANTs and the centric-based controller are developed for boost converters. The obtained results confirm the enhanced dynamic response and fixed frequency operation as natural advantages of the proposed control scheme.

The theoretical findings are supported by detailed mathematical procedures and validated by experimental results, which highlight the practical usefulness of the concepts introduced in this work.

Preface

This work is based on research performed at the Electrical and Computer Engineering department of the University of British Columbia by Ignacio Galiano Zurbriggen, under the supervision of Dr. Martin Ordonez. Some experimental validation work was done in collaboration with Matias Anun.

Versions of chapter 2 and 3 have been published at the IEEE Applied Power Electronics Conference and Exposition (APEC), 2013 [1, 2].

An extended version of chapter 3 has been submitted to a power electronics journal [3].

A version of chapter 4 has been submitted to a conference in power electronics [4].

As first author of the above-mentioned publications, the author of this thesis developed the theoretical concepts and wrote the manuscripts, receiving advice and technical support from Dr. Martin Ordonez, and developed simulation and experimental platforms, receiving contributions from Dr. Ordonez's research team, in particular from the MASc. student Matias Anun who developed some specific experimental tasks.

Table of Contents

Abstract ii

Preface iv

Table of Contents v

List of Tables viii

List of Figures ix

Acknowledgements xii

Dedication xiii

1 Introduction 1

1.1 Motivation 1

1.2 Literature Review 3

1.2.1 Dynamic Physical Limits of Performance 3

1.2.2 Control for Buck Converters 5

1.2.3 Control for Boost Converters 6

1.3 Contribution of the Work 9

1.4 Thesis Outline 11

2 Dynamic Physical Limits of Buck Converters: the $T_0/4$ Transient Benchmark Rule 13

2.1 Buck Transient Natural Trajectories and Response 14

2.2 Buck Loadability and Sudden Load Transients 18

2.2.1 Loading 20

2.2.2 Unloading 22

2.3 Benchmarking Procedure Example 24

2.4 Experimental Results 26

2.5 Summary 28

3 Average Natural Trajectories (ANTs) for Buck Converters: Centric-Based Control 30

3.1 Buck Converter Ideal ANTs Derivation 32

3.2 Approaching the Target 38

3.3 Closing the Loop with a Centric-Based Controller 40

3.3.1 Periodic Center Calculation 42

3.3.2 Domain Restrictions 42

3.3.3 Steady State Error Correction 42

3.4 Experimental Results 44

3.5 Comparison with Linear Controllers 45

3.6 Tolerances Sensitivity Analysis 49

3.7 Buck Converter Non-Ideal ANTs Derivation 52

3.8 Closed-Loop Controller Including Estimation of Parasitics 56

3.9 Centric Controller Benchmark 59

3.10 Summary 61

4 Average Natural Trajectories (ANTs) for Boost Converters: Centric-Based Control 63

4.1 Normalized Boost Converter ANTs Derivation 65

4.2 Approaching the Target 69

4.3 Closing the Loop with a Centric-Based Controller 71

4.4 Experimental Results 72

4.5 Summary 74

5 Conclusions 76

5.1 Summary 76

5.2 Future Work 77

Bibliography 78

List of Tables

1.1 Some theoretical limits 4

2.1 Buck converter parameters 24

3.1 Buck converter parameters 45

3.2 Main parasitics 45

3.3 Centric - linear controllers comparison 47

3.4 Centric controller parameter deviations 50

4.1 Boost converter parameters 74

4.2 Main parasitics 74

List of Figures

1.1 Controls in power electronics 2

1.2 Centric-based, sliding-mode and dual-loop linear controllers in buck converters: a conceptual comparison. 8

1.3 Normalized buck converter 10

1.4 Normalized boost converter 11

2.1 Normalized buck converter 14

2.2 Start-up transient in geometrical and time domains. 15

2.3 Loading transient represented on geometrical and time domains. 19

2.4 Normalized loading transient parameters as function of V_{ccn}, using Δi_{loadn} as parameter a) voltage drop $\Delta v_{on(min)}$ b) minimum loading recovery time $t_{recn(min),Loading}$ 21

2.5 Unloading transient represented on geometrical and time domains. 23

2.6 Comparison between physical limit operation and traditional compensation techniques. 25

2.7 Start-up experimental results for a) low step-down ($V_{ccn} = 1$) and b) high step-down $V_{ccn} = 10$ transients. 27

2.8 Start-up, loading and unloading transients for $V_{ccn} = 2$. 28

3.1 a) Normalized PWM driven buck converter. b) Pseudo-ideal natural trajectory forced in a real converter. 32

3.2 Ideal PWM natural trajectory with $V_{ccn} = 2$, $d = 0.5$ and $f_{sn} = 10$. 33
3.3 Several PWM-driven buck converter ANTs departing from unique initial operating point. 36
3.4 Ideal fixed duty cycle target approaching method for different initial conditions 39
3.5 Fixed duty cycle target approaching method forced in a real converter 40
3.6 Centric-based controller: a) scheme, and b) experimental results. 41
3.7 Closed-loop controller concept 43
3.8 Comparison between dual-loop linear and centric-based controllers. Start-up transient for a) linear, and b) centric-based. 46
3.9 Comparison between dual-loop linear and centric-based controllers. Loading/unloading transients with $\Delta i_{on} = 1$ for a) linear, and b) centric-based. . 47
3.10 Comparison between dual-loop linear and centric-based controllers. Loading/unloading transients with $\Delta i_{on} = 0.5$ for a) linear, and b) centric-based. 48
3.11 Centric-based controller performance under parameter deviations. Start-up, loading and unloading transients for a) $L_{real} = 0.8\ L$, $C_{real} = 0.8\ C$; and b) $L_{real} = 0.8\ L$, $C_{real} = 1.2\ C$; 50
3.12 Centric-based controller performance under parameter deviations. Start-up, loading and unloading transients for a) $L_{real} = 1.2\ L$, $C_{real} = 0.8\ C$; and b) $L_{real} = 1.2\ L$, $C_{real} = 1.2\ C$. 51
3.13 a) Non-ideal normalized PWM driven buck converter. b) Real PWM natural trajectory. 52
3.14 Non-ideal natural trajectory with $V_{ccn} = 2$, $d = 0.5$ and $f_{sn} = 10$. 54
3.15 Centric-based controller with load current estimation: a) scheme, and b) experimental results. 57
3.16 Response of the centric-based controller with load current measurement for loading/unloading transients with $\Delta i_{on} = 1$ (a), and $\Delta i_{on} = 0.5$(b). 59

3.17 Performance comparison between the ideal centric-based controller and the dynamic physical limits. 60

4.1 a) Normalized PWM driven boost converter. b) PWM natural trajectories in a real converter. 64

4.2 Ideal natural trajectories with $V_{ccn} = 0.5$, $d = 0.5$ and $f_{sn} = 10$. 66

4.3 Several PWM-driven boost converter ANTs departing from unique initial operating point. 68

4.4 Fixed duty cycle target approaching method for different initial conditions . 70

4.5 Centric-based controller experimental results. a) Open-loop with duty cycle precalculation. b) Closed-loop response for start-up, loading and unloading transients. 73

Acknowledgements

I would like to sincerely thank my supervisor Dr. Martin Ordonez for accepting me as part of his research team. His support, extreme dedication and valuable technical advice during my Master's program are greatly appreciated.

I would also like to acknowledge my lab mates, the research team, for kindly sharing his experience and knowledge and for making of these years an enjoyable experience beyond technical aspects.

I must thank the professors of the courses I took as part of the program for the valuable knowledge transferred, and the staff of the Electrical and Computer Engineering department of the University of British Columbia for their assistance in academic matters.

I feel the need to express my deepest gratitude to my girlfriend Silvita, to my parents Ana and Ernesto, to my brothers Alejandro, Federico, and Santiago, and to my closest friends, for their constant encouragement and moral support without which this work would not have been possible.

My English teachers deserve to be mentioned as well for having taught me the language in a very short period of time and almost from scratch.

Last but not least, I would like to thank you, the reader, for showing interest in this work.

To those in my deep love and respect

Chapter 1

Introduction

1.1 Motivation

Switching power converters are present in almost every electrical/electronic device in today's world. The ever-increasing demand of higher power densities (reduced size for the same power) and higher efficiencies, has turned power electronics ubiquitous in any apparatus. The applications range from mass-produced low power converters (mili Watts) used in portable devices (ie: cell-phones, digital cameras, music/video players, etc.) to high power (Mega Watts) applications produced on a small scale for use in power distribution.

Closed-loop controllers are usually implemented in power conversion systems in order to obtain a tight regulation of the output variables at the desired values. Controllers are the 'brain' of the system, and the performance of the converters is strongly related to them. Higher efficiency, better performance, smaller size and reduced cost can be reached just by improving the controllers. Among the main aspects that determine the performance of power converter control schemes, dynamic response and robustness are undoubtedly two of the most important.

The dynamic response of a power converter is characterized by two main parameters: recovery time and peak deviations in the state variables. The recovery time is given by the period of time the converter takes to reach steady state after a change in the operating conditions, for instance a step-up in the load current. The deviations in the converter state variables during a transient determine how much the voltages and currents differ from the

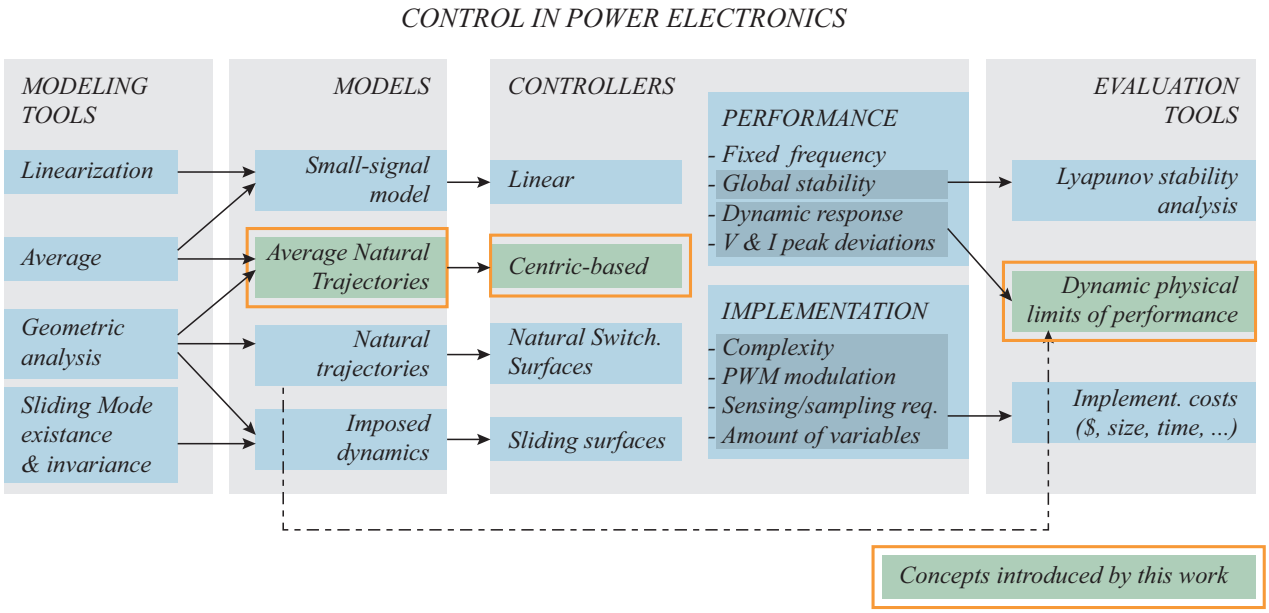

Figure 1.1: Controls in power electronics

desired steady state values, and the peak values reached can determine whether or not the converter is suitable for a determined application. For instance, an electronic system that requires a 3.3 V power supply might require a recovery time of 1 ms and a maximum drop of 0.3 V in order to function properly. Undesired saturation in magnetic elements due to large current peaks, and system failures due to large and maintained voltage drops can be avoided by implementing controllers featuring fast and predictable dynamic response.

The robustness of a system is defined as its ability to deal with external and/or internal disturbances. Tolerances in the converter components and inaccuracies of the models employed are some of the factors that can cause unstable behaviours in power converters. Taking these effects into account when designing the controllers is essential to guarantee a reliable operation during transients and in steady state.

Other features related to the implementation, such as complexity, constant switching frequency operation, and sensing/sampling requirements, are very important as well, since they define the amount of resources required by the controller, and how well it can be implemented using technologies currently available.

1.2 Literature Review

Characteristic features of the different control techniques are strongly related to the models employed for their design, which inherently depend on the mathematical tools by means of which they have been developed. An illustrative sketch including some of the most popular schemes and models is provided in Fig. 1.1.

Linear compensators based on small-signal averaged models have been the preferred alternative for controlling power converters during the last four decades. Although proven to be effective by countless industrial applications, these control techniques present issues related to the model employed, which is based on a local linearization and therefore is only valid in the neighborhood of a determined operating point.

Nonlinear solutions of many different natures have been proposed, resulting in substantial improvements to the robustness and dynamic response, boundary controllers being one of the most popular alternatives.

However, the improvements cannot be properly quantized due to a lack of awareness about the limits of performance limits of the converters. The following literature review goes through the efforts that, during many years, have been made to find a controller performance benchmark tool for buck converters and to improve controllers for basic Buck and Boost DC-DC topologies.

1.2.1 Dynamic Physical Limits of Performance

With over 5,000 buck control related papers available at IEEE Xplore (2013), the engineering and scientific community has been looking for ways to improve the dynamic performance of buck derived topologies for decades, either by developing new models and implementing new control techniques [5–19] or by introducing modifications to the topology [20–24]. Many other disciplines follow the same trend, such as electrochemistry in the search for fuel cell

Table 1.1: Some theoretical limits

DEVICE	THEORETICAL LIMIT
Wind Turbine	59.3% effic. (Betz law)
Fuel Cell	$1.23V$ (Nernst cell voltage)
Solar Cell	33.7% effic. (Shockley-Queisser Limit)
Lithium-Ion Battery Cell	$4.1V$ $100Ah/Kg$ capacity
Class A Audio Amplifier	25% effic.
Buck converter, high step-down ($v_{in}/v_{out} \to \infty$)	$\boldsymbol{To/4}$ **[s]** start-up transient
Buck converter, low step-down ($v_{in}/v_{out} = 1$)	$\boldsymbol{To/3}$ **[s]** start-up transient

voltages closer to the theoretical limit of 1.23V (Nernst voltage), or the improvement of solar cells efficiency in the attempt to reach values closer to the theoretical maximum of 33.7% (Shockley-Queisser limit); the pursuit of higher efficiencies in wind turbines in order to approach the theoretical maximum of 59.3% (Betz law); and the improvement of steam and Diesel engines to obtain efficiency values closer to the theoretical maximums (given by Carnot and Diesel cycles respectively) in mechanical engineering (Table I). Unlike these disciplines, power electronic engineers/researchers do not use the theoretical limits of performance to benchmark controllers. Unfortunately, the relative gains or improvements to the dynamic response of the converter cannot be fully determined if the results are not compared with the theoretical transient time limits.

Transient analysis of buck converters has been performed in the past using small-signal modeling [25]. Due to constraints of small-signal analysis, the results do not provide any

information about performance limits. Critical parameters on the transient response and their effects have been also analyzed [26–28]. However, the theoretical minimum transient times are not specifically addressed. Based on small-signal analysis, an effort to establish a benchmark system using a standard 20W converter design was proposed [29], but the physical limits of the system are not discussed. Later interesting work used simulations and experimental results to explore the limits of buck performance [30–33], presenting advancements to the field. The derivations and general expressions necessary to determine the theoretical physical limits remained unaddressed and without a concrete solution. In fact, rather than being common knowledge, the theoretical transient limits of buck converters remains unknown to technical experts, power designers, the power conversion community in general.

1.2.2 Control for Buck Converters

Using linear control techniques in buck topologies, switching and sampling frequencies are kept constant and robust systems can be obtained by performing stability analysis and tuning the compensator parameters [34–42]. However, the dynamic performance can be improved to only a limited extent and, since the models of the converter are only valid for small-signal variations, the controllers perform poorly under large load transients. Linear/non-linear alternatives based on output capacitor current of the buck converter have been proposed in [43–45], where non-linear solutions provide improvements in the dynamic response while classical linear controllers are used for steady-state regulation.

Among the non-linear techniques, boundary controllers are a popular alternative for controlling buck converters. Typically, the main advantage of this type of controllers is its fast and predictable transient response, which in some cases reaches the physical limit of performance [1]. Conceptual boundary controlled systems are bounded stable by nature, as long as the sliding mode existence and invariance conditions are met [46, 47]. Chattering and variable switching frequency are the major issues they present [48–50]. Several techniques

to obtain constant switching frequencies for first and second order switching surfaces have been successfully implemented [51–55]. Since the solution deviates from the ideal concept, unboundedness and steady state error become an issue. A different situation takes place in the case of natural switching surfaces of buck converters, where the ideal behavior is bounded stable, the steady state switching frequency is fixed and large transients are solved in only one switching action [33, 56–58]. However, there are real factors that prevent the converter from exhibiting ideal behavior, and therefore the robustness of the system results highly dependent on factors like finite sampling frequency, reactive components value accuracies and losses effect.

1.2.3 Control for Boost Converters

Fixed frequency operation and a reliable steady state behaviour can be achieved in boost topologies by using traditional linear controllers. However, due to the characteristic right half plane zero (RHPZ) of the small signal control-to-voltage transfer function, the robust controllers that can be designed present low bandwidth, which leads to a sluggish dynamic response [59]. Introducing a second loop to control the inductor current certainly allows an increase in the controller bandwidth [41, 60, 61]. Nevertheless, the RHPZ is not eliminated and therefore the dynamic response is still limited. Besides, since the employed models are only valid for small signal, the response under large transients cannot be predicted and large-signal stability cannot be ensured. Several approaches to solve this last issue in the implementation of small-signal based controllers have been presented recently [38, 62–68]. Although interesting results are obtained, the complexity of the implementation is greatly increased and the dynamic performance is still limited due to the nature of the models employed.

Non-linear geometric-based approaches present an appealing alternative for boost con-

verters, where the effect of the characteristic non-minimum phase behaviour is eliminated since the control decisions are based purely on the system operating point. First order switching surface controllers are a popular alternative in which a predictable response is obtained once the sliding mode is reached [46–49]. Unpredictable current peaks before reaching sliding mode, steady state error, chattering and variable switching frequency are some of the issues in the implementation of this technique. Although successful attempts to solve most of these issues have been presented [55, 69, 70], the simplicity of the original concepts is compromised. Using Second order switching surfaces, the dynamic response can be improved while the achievement of constant switching frequencies can be maintained [52, 71]. Besides the increase in complexity needed to obtain constant frequency, overshoot and large current spikes during large transients are some of the disadvantages the technique presents.

The physical limit of dynamic performance of boost topologies is reached by boundary controllers using the Natural Switching Surfaces, which have been proven to be successful in several DC-DC topologies. Fixed frequency steady state operation and a predictable time-optimal transient solution performing only one switching action are the main advantages of this technique [1, 33, 57, 58, 72, 73]. On the other hand, large current peaks are needed to achieve the physical limit of dynamic performance; high sampling frequencies are required and the robustness of the system is tied to values accuracy and losses effect in the reactive components. As a result, the technique presents an excellent alternative in high-power applications where the high-end requirements for the controller implementation are justified by the obtaining of time-optimal dynamic performance and the minimization of the number of switching actions.

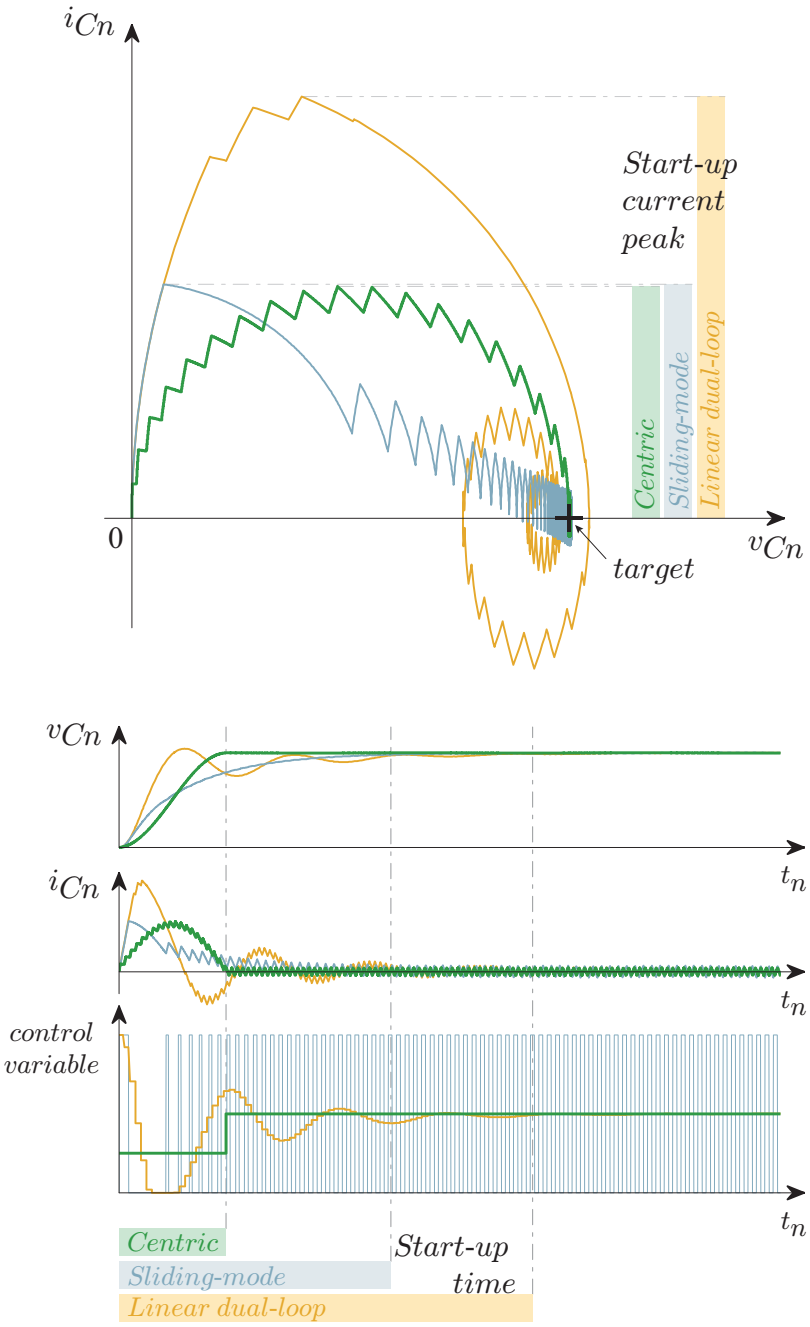

Figure 1.2: Centric-based, sliding-mode and dual-loop linear controllers in buck converters: a conceptual comparison.

1.3 Contribution of the Work

This work introduces valuable theoretical concepts to the field of controls for power electronics systems as well as useful practical applications of the ideas developed:

- The first concept comes after a clear need identified in the literature review: a benchmark tool to objectively assess the dynamic performance of power electronics controllers. The dynamic physical limits of performance are introduced as a theoretical optimal response only achievable in ideal conditions, which cannot be exceeded.

- Second, a novel way of modeling power converters that merges geometrical analysis with traditional averaging techniques, is introduced: the Average Natural Trajectories (ANTs). The proposed model accurately describes the averaged large-signal behaviour of PWM-driven power converters.

- Third, based on the obtained ANTs, the novel geometric-based control technique illustrated in Fig. 1.2 referred to as centric-based control. The proposed technique features repeatable and predictable dynamic response reaching values close to the theoretical limit of performance, while the complexity of the implementation is kept low, filling the gap between small-signal-based linear controllers and geometric-based boundary techniques. As shown in the conceptual figure, the proposed scheme features shorter transient times and lower peak current than two of the most popular techniques in the field, linear and sliding mode controllers.

It is worth mentioning that the ideas introduced in this work can be applied to other switching power converter topologies, and since the analysis is performed in a normalized fashion, the results are valid for any combination of values of the reactive components.

As part of the focus of this work, a geometrical description of the theoretical optimal response of the normalized buck converter illustrated in Fig. 1.3 is obtained. Analyzing

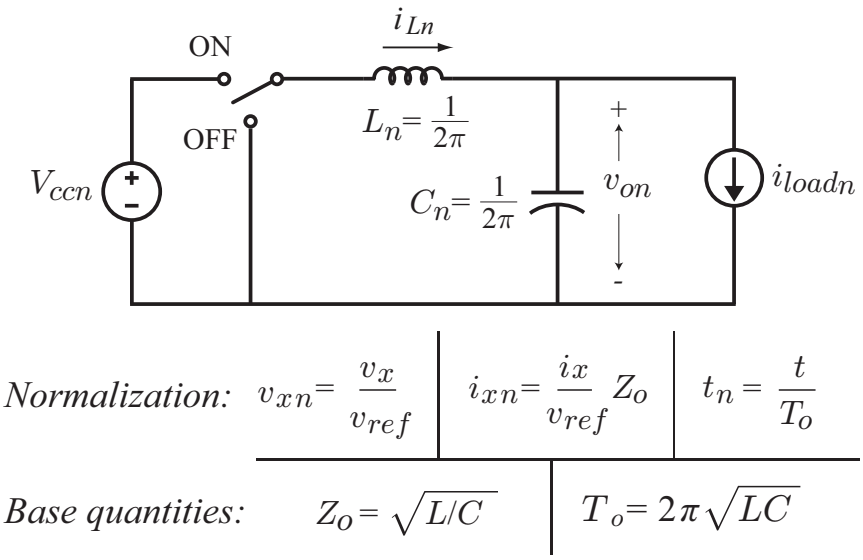

Figure 1.3: Normalized buck converter

the optimal response, closed-form equations that determine the physical limits of dynamic performance of buck converters are derived and the $T_0/4$ start-up transient rule is derived, setting a strong benchmarking point.

The Average Natural Trajectories are derived for buck converters and based on the model obtained, the centric-based control is implemented. The enhanced dynamic response predicted is validated by experimental results. In order to illustrate that the concepts introduced in this work can be developed for any other topology, and due to the outstanding performance obtained by the centric-based controller implementation, the analysis is extended to boost converters. The large-signal model is obtained by deriving the ANTs in the normalized converter shown in Fig. 1.4, and the controller is implemented in an experimental platform, obtaining excellent results. The controllers are implemented in low-cost DSPs, which makes the technique suitable for implementation in large-scale production converters, highlighting the important contribution of the work to the practical field.

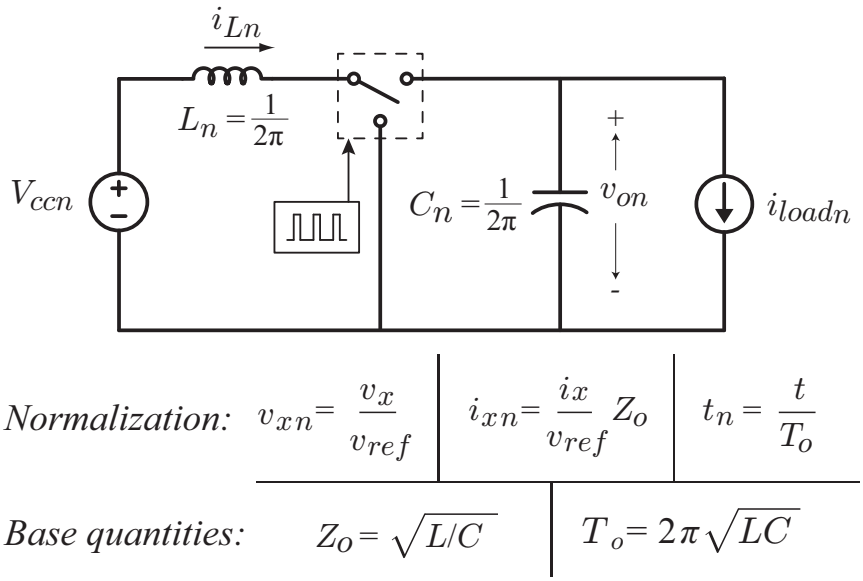

Figure 1.4: Normalized boost converter

1.4 Thesis Outline

This work is organized in the following manner:

- In chapter 2, the buck converter physical limits of performance are developed. A normalization procedure is applied to the buck converter state equations to obtain expressions that are not dependent on the system parameters. These expressions are solved in time domain first, and then merged to obtain a geometric representation of the converter behaviour for ON and OFF states, which defines the converter natural trajectories. Using the insight provided by the trajectories, the theoretical optimal response is found in a geometric domain, and characterized by mathematical expressions for three types of transient: start-up, loading and unloading. A benchmark procedure is introduced, in order to address the practical contribution of the concepts developed in this work. The findings are validated using simulations and experimental results in order to illustrate the different transients analyzed.

- In chapter 3, the concepts of Average Natural Trajectories (ANTs) and centric-based controls are developed for buck converters. The normalization of the ON and OFF state equations of buck converters is followed by an average procedure to obtain an averaged representation of the converter behaviour. The average state equations are obtained and solved in time domain to find expressions that describe the averaged evolution of PWM driven buck converters. The time-domain expressions are combined to obtain trajectories that model the natural evolution of the buck converter variables in a geometric domain: the Average Natural Trajectories (ANTs) are obtained for buck converters. Based on the derived large-signal model, the centric-based controller is conceptually derived for buck converters. Simulation and experimental results are shown in order to validate the enhanced dynamic performance of the proposed technique.

- In chapter 4, the concepts of Average Natural Trajectories (ANTs) and centric-based controls are introduced for boost converters. The ON and OFF state equations of boost converters are normalized and averaged over a switching period in order to obtain a set of duty-cycle dependent state equations that describe the behaviour of PWM driven boost converters. The averaged equations are solved in time domain, obtaining a description of the natural evolution of the averaged variables. The averaged time-domain equations are combined to obtain the Average Natural Trajectories of boost converters, which models the large-signal behaviour in a geometric domain.

- Finally, in chapter 5 a summary and conclusions of this work are presented along with an account of work under development and ideas for future research.

Chapter 2

Dynamic Physical Limits of Buck Converters: the $T_0/4$ Transient Benchmark Rule

As identified in the literature review, and unlike researchers in other disciplines, the designer of power converter controls does not count with a tool that helps him/her to determine how important the improvements under development are. Furthermore, since the analysis is not usually performed in the normalized domain, there is no clear indication of how well the controller performs and how much better it could for the reactive components being used.

It is the aim of this chapter to introduce the concepts of normalized analysis and physical limits of performance, and to present the way in which these can be used as a tool to to enable the objective evaluation of the performance of different control techniques.

This chapter presents the derivation and final equations of the theoretical performance limits of buck converters and validates the findings with experimental results - a valuable design benchmark for power engineers and researchers. The theoretical optimal behavior is fully characterized in the normalized domain and the findings are valid and general for any combination of specifications. As a result, the $T_0/4$ rule (quarter of the filter natural period) is obtained, providing a remarkably useful benchmark equation. In addition, through this work, power designer and researchers are equipped with a set of transient response limits to aid filter design tasks and controller performance comparisons.

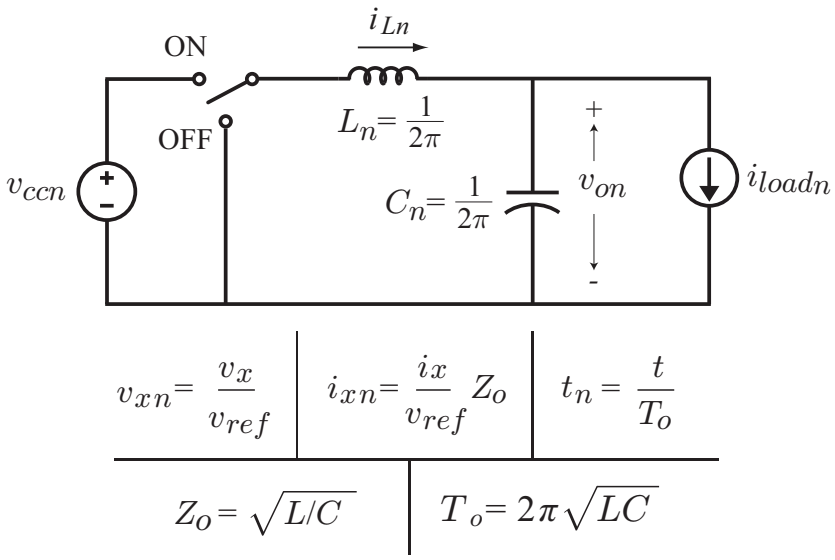

Figure 2.1: Normalized buck converter

Fig. 2.2 shows the conceptual start-up evolution of a buck converter in a normalized phase-plane. The figure illustrates the three critical points (normalized) of the ideal theoretical transient trajectory: turn on action ❶, turn off action ❷, and arrival to target point ❸. Fig. 2.7 shows the resulting experimental test to confirm the transient response limits for (a) low step down ratio $V_{ccn} = 1$ and (b) high step down ratio $V_{ccn} = 10$.

2.1 Buck Transient Natural Trajectories and Response

In order to add generality to the analysis, a normalized buck is employed for the derivation leading to the elimination of the inductor and capacitor filter values, output voltage, power rating, input voltage, and time domain. The resulting normalized model is valid for any combination of filter component values.

The normalization:

$$t_n = \frac{t}{T_0}; \qquad Z_{xn} = \frac{Z_x}{Z_0}; \qquad v_{xn} = \frac{v_x}{v_{ref}}; \qquad i_{xn} = \frac{i_x}{i_{ref}}$$

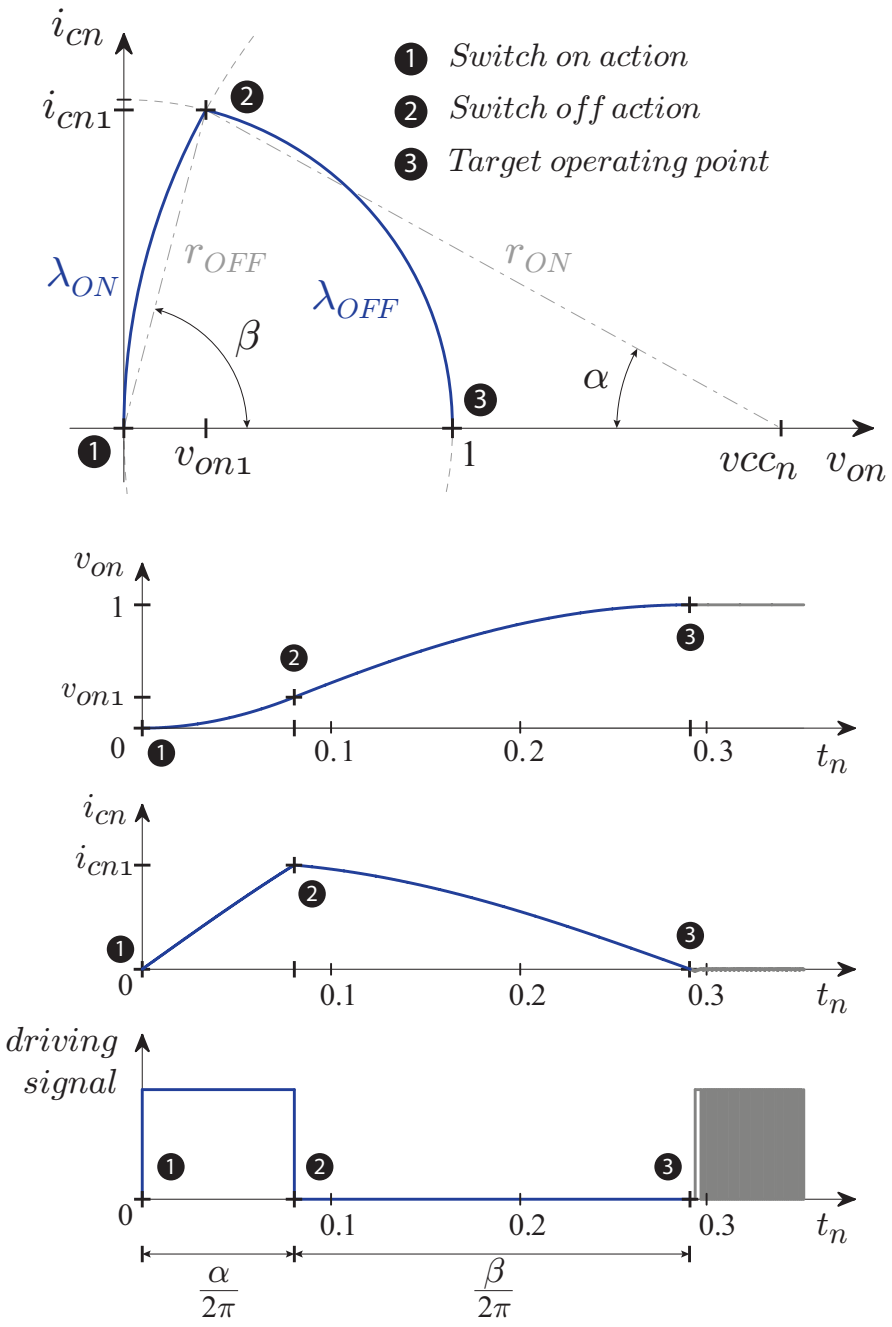

Figure 2.2: Start-up transient in geometrical and time domains.

is performed using as base quantities the filter characteristic impedance and resonance period and the reference voltage and current:

$$Z_0 = \sqrt{L/C}; \qquad T_0 = 2\pi\sqrt{LC}; \qquad v_{ref}; \qquad i_{ref} = \frac{v_{ref}}{Z_0};$$

The differential equations that characterize the response of buck converters can be expressed as:

$$C\frac{dv_o}{dt} = i_L - i_o \tag{2.1}$$

$$L\frac{di_L}{dt} = u\ V_{cc} - v_o \tag{2.2}$$

where u takes the values 1 and 0 for ON and OFF states respectively.

Performing the normalization, they become:

$$\frac{1}{2\pi}\frac{dv_{on}}{dt_n} = i_{Ln} - i_{on} \tag{2.3}$$

$$\frac{1}{2\pi}\frac{di_{Ln}}{dt_n} = u\ V_{ccn} - v_{on} \tag{2.4}$$

Solving them, time domain expressions that determine the evolution of capacitor voltage and inductor current are found:

$$v_{on}(t_n) = [v_{on}(0) - u\ V_{ccn}]cos(2\pi t_n) + [i_{Ln}(0) - i_{on}]sin(2\pi t_n) + u\ V_{ccn} \tag{2.5}$$

$$i_{Ln}(t_n) = [i_{Ln}(0) - i_{on}]cos(2\pi t_n) + [v_{on}(0) - u\ V_{ccn}]sin(2\pi t_n) + i_{on} \tag{2.6}$$

The capacitor current is derived from (2.6):

$$i_{Cn}(t_n) = [i_{Ln}(0) - i_{on}]cos(2\pi t_n) - [v_{on}(0) - u\ V_{ccn}]sin(2\pi t_n) \tag{2.7}$$

By combining (2.5) and (2.7), the time can be eliminated, obtaining the equivalent of the buck in the geometrical domain defined by v_{on} and i_{Cn}:

$$\lambda_{ON} : i_{cn}^2 + (v_{on} - V_{ccn})^2 - i_{cn}^2(0) - (v_{on}(0) - V_{ccn})^2 = 0 \tag{2.8}$$

$$\lambda_{OFF} : i_{cn}^2 + v_{on}^2 - i_{cn}^2(0) - v_{on}^2(0) = 0, \tag{2.9}$$

which are the natural circular trajectories moving at the angular speed $\omega_{on} = 2\pi$.

Since the aim of this work is to find the theoretical physical limits on the dynamic performance of buck converters, the paths that the operating point follows are determined by the ON and OFF natural trajectories (λ_{ON} and λ_{OFF}). The normalized angular speed at which the operating point is moving is constant; therefore the transient times can be determined by calculating the angles of the operating point circular paths required to reach the target located at $v_{on} = 1$ and $i_{cn} = 0$, as depicted in Fig. 2.2.

At the initial instant ❶ in Fig. 2.2, the switch is turned on and the operating point follows the λ_{ON} trajectory covering the angle α. Thereafter, at the instant ❷, the λ_{OFF} state Natural Trajectory is followed (the switch is turned off), moving toward the target point and covering the angle β. Finally, the target operating point is reached at ❸.

By performing a geometrical analysis described above, the normalized start-up transient analytical equation is obtained as follows:

$$t_{start_n} = \frac{\alpha + \beta}{2\pi} \tag{2.10}$$

where

$$\alpha = cos^{-1}\left(1 - \frac{1}{2\ V_{ccn}^2}\right), \tag{2.11}$$

and

$$\beta = cos^{-1}\left(\frac{1}{2\ V_{ccn}}\right) \tag{2.12}$$

As can be seen in (2.10)-(2.12), the start-up physical limit transient time (normalized) depends only on the normalized input voltage ($V_{ccn} = V_{cc}/v_{ref}$) - no other parameter is involved. The resulting representation is remarkably simple and provides extraordinary insight into the transient evolution. By using (2.10)-(2.12), the minimum theoretical normalized start-up transient time (t_{start_n}) can be found for any input-to-output voltage ratio. For example, the absolute limit of operation for a buck converter occurs when the input voltage is much greater than the output voltage $V_{ccn} >> v_o$ (or $V_{ccn} \to \infty$), yielding a total minimum theoretical transient time $t_{start_n} = 1/4$. By denormalizing, the rule of:

$$t_{start(min)} = T_0/4 = \frac{\pi}{2}\sqrt{LC} \tag{2.13}$$

is established, where T_0 is the natural resonant period of the output filter. Equation (2.13) is referred to as the quarter of the filter natural period rule, and represents the absolute physical limit of the system. On the other extreme, when $V_{cc} = vo$ (or $V_{ccn} = 1$) the transient time is given by $t_{start_n} = 1/3$ (normalized) or $T_0/3$ in the time domain. The experimental captures depicted in Fig. 2.7 provide experimental validation for both cases, low step-down and high step-down, respectively.

2.2 Buck Loadability and Sudden Load Transients

These transients are produced once the system is in steady state, by adding or removing load. Steps up (loading) and down (unloading) in the load current, of a magnitude Δi_{loadn}, are used for the analysis. Representations of the loading and unloading transients in both domains (geometrical and time) are shown theoretically in Figs. 2.3 and 2.5, and experimentally in Fig 2.8. In both cases of analysis, the initial operating point is defined when the load step occurs.

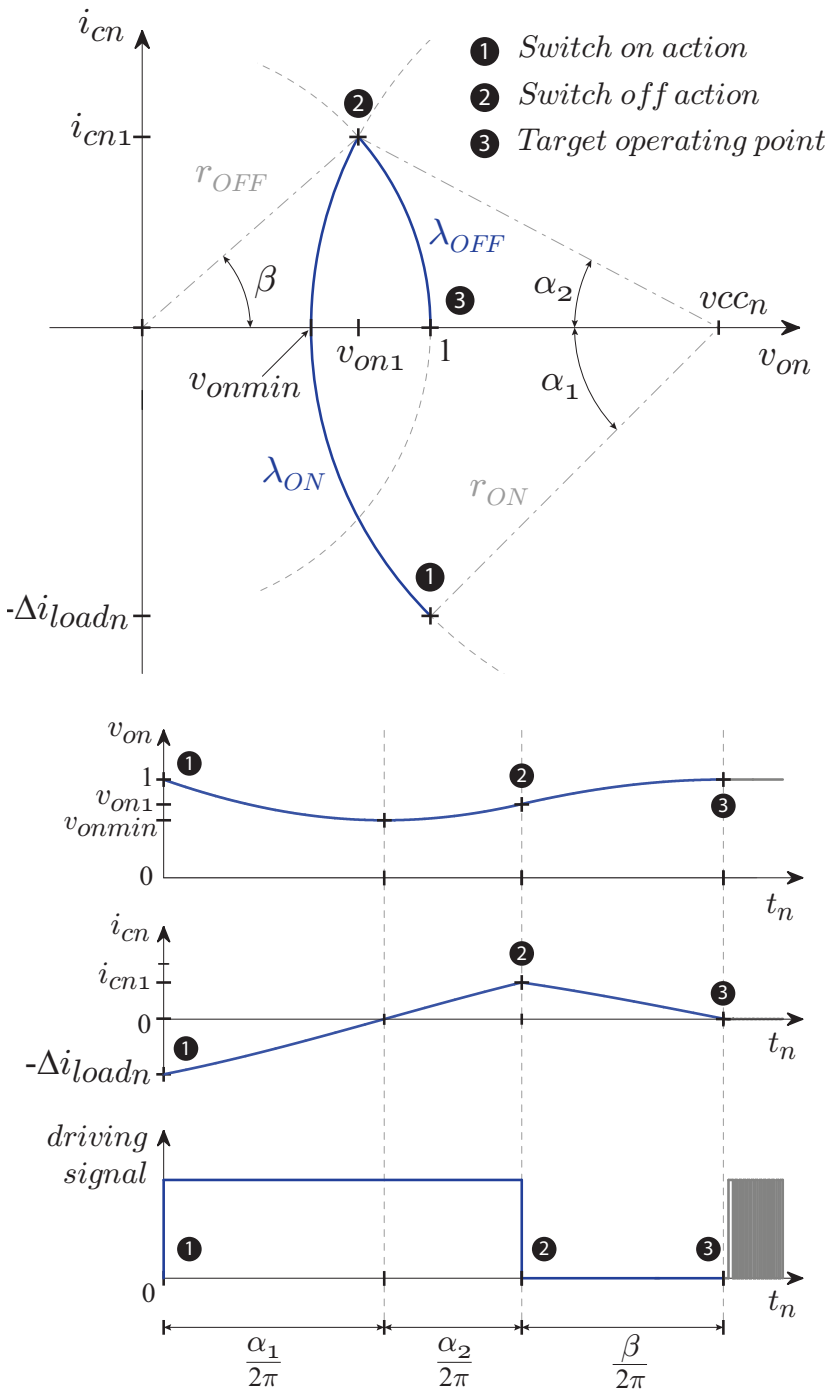

Figure 2.3: Loading transient represented on geometrical and time domains.

2.2.1 Loading

In Fig. 2.3, the loading transient is shown in the geometrical and time domains, where the initial operating point ❶ is located at $(1; -\Delta i_{loadn})$. At the zero instant, the switch is turned on and the operating point starts to follow the λ_{ON} trajectory. It remains in that state until the λ_{OFF} trajectory that contains the target operating point (for $i_{cn} > 0$) is reached at ❷. The operating point first covers the angle α_1 to reach the zero current intersection, and then it continues moving through α_2 to reach ❷. The switch is turned off at ❷ and the operating point covers the angle β to reach the target ❸. By performing a geometrical analysis of the loading transient (Fig. 2.3) the angles α_1, α_2 and β are found:

$$\alpha_1 = tan^{-1}\left(\frac{\Delta i_{loadn}}{V_{ccn} - 1}\right) \tag{2.14}$$

$$\alpha_2 = tan^{-1}\left(\frac{\Delta i_{loadn}\sqrt{4\ V_{ccn} - {\Delta i_{loadn}}^2}}{2\ V_{ccn}^2 - 2\ V_{ccn} + {\Delta i_{loadn}}^2}\right) \tag{2.15}$$

$$\beta = tan^{-1}\left(\frac{\Delta i_{loadn}\sqrt{4\ V_{ccn} - {\Delta i_{loadn}}^2}}{2\ V_{ccn} - {\Delta i_{loadn}}^2}\right) \tag{2.16}$$

And, since the angular speed is $\omega_{on} = 2\pi$, the normalized theoretical minimum recovery time is given by:

$$t_{recn(min),Loading} = \frac{\alpha_1 + \alpha_2 + \beta}{2\pi} \tag{2.17}$$

By using (2.17), the minimum recovery time for any loading transient can be calculated to establish a benchmark recovery.

Since the analysis is performed in the geometrical domain, the transient can be fully characterized, and particular aspects can be analyzed. One of the parameters of interest is the theoretical minimum voltage drop (dynamic regulation), which given by:

$$\Delta v_{on(min)} = 1 - V_{ccn} + \sqrt{(V_{ccn} - 1)^2 + {\Delta i_{loadn}}^2} \tag{2.18}$$

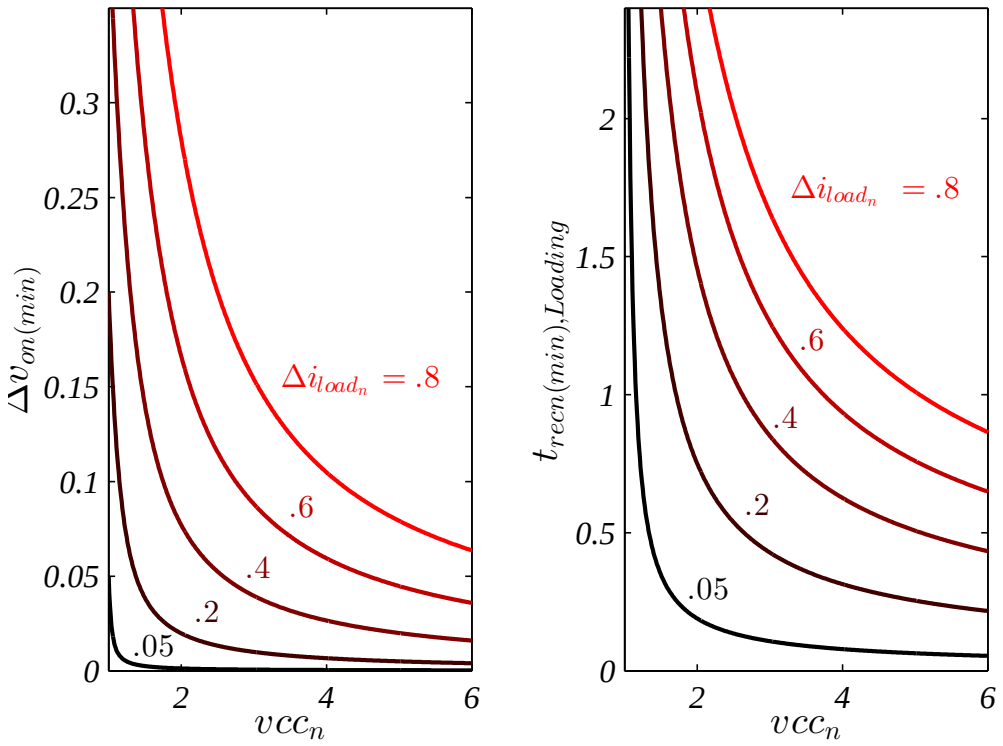

Figure 2.4: Normalized loading transient parameters as function of V_{ccn}, using Δi_{loadn} as parameter a) voltage drop $\Delta v_{on(min)}$ b) minimum loading recovery time $t_{recn(min),Loading}$

The values of time recovery and voltage drop are general and valid for any combination of parameter, and are synthesized in two normalized plots shown in Fig. 2.4 (a) and (b). These plots allow the power electronics designer to find the theoretical minimum recovery time and voltage drop for any load current step-up in a fast manner. Normalizing the current step and determining the converter input to output voltage ratio are the only previous steps needed to read the optimal values from the plots. For instance, if a current step-up of a normalized magnitude $\Delta i_{loadn} = 1$ happens in a normalized buck converter with $V_{ccn} = 2$, the theoretical minimum recovery time and voltage drop are $t_{recn(min),Loading} = 0.3175$ and $\Delta v_{on(min)} = 0.4142$.

2.2.2 Unloading

The unloading transient is shown in Fig. 2.5. The initial operating point ❶ is located at $(1; \Delta i_{loadn})$. At the zero instant, the switch is turned off and the operating point moves following the trajectory λ_{OFF}, covering the angle β_1 to reach the maximum voltage point (v_{onmax}) and β_2 to reach the switching point ❷. At that moment, the switch is turned on and λ_{ON} is followed during the angle α to reach the target operating point ❸.

Performing geometrical analysis, the normalized minimum recovery time for unloading transients is found:

$$t_{recn(min),Unloading} = \frac{\beta_1 + \beta_2 + \alpha}{2\pi}; \tag{2.19}$$

where:

$$\beta_1 = tan^{-1}\left(\Delta i_{loadn}\right) \tag{2.20}$$

$$\beta_2 = tan^{-1}\left(\frac{\Delta i_{loadn}\sqrt{4\ V_{ccn}(V_{ccn}-1) - {\Delta i_{loadn}}^2}}{2\ V_{ccn} + {\Delta i_{loadn}}^2}\right) \tag{2.21}$$

$$\alpha = tan^{-1}\left(\frac{\Delta i_{loadn}\sqrt{4\ V_{ccn}(V_{ccn}-1) - {\Delta i_{loadn}}^2}}{2\ V_{ccn}^2 - 2\ V_{ccn} - {\Delta i_{loadn}}^2}\right) \tag{2.22}$$

The expression that defines the theoretical minimum overshoot voltage is found by analyzing the evolution of the variables in the geometrical domain:

$$v_{onmax} = \sqrt{1 + {\Delta i_{loadn}}^2} \tag{2.23}$$

This simple equation, indicates the normalized minimum value that the output voltage reaches during a load current step-down transient, as function of normalized step magnitude only. The effectiveness of the controller to avoid overshoot during this kind of transients can be objectively assessed by comparing the obtained values with the theoretical minimum presented.

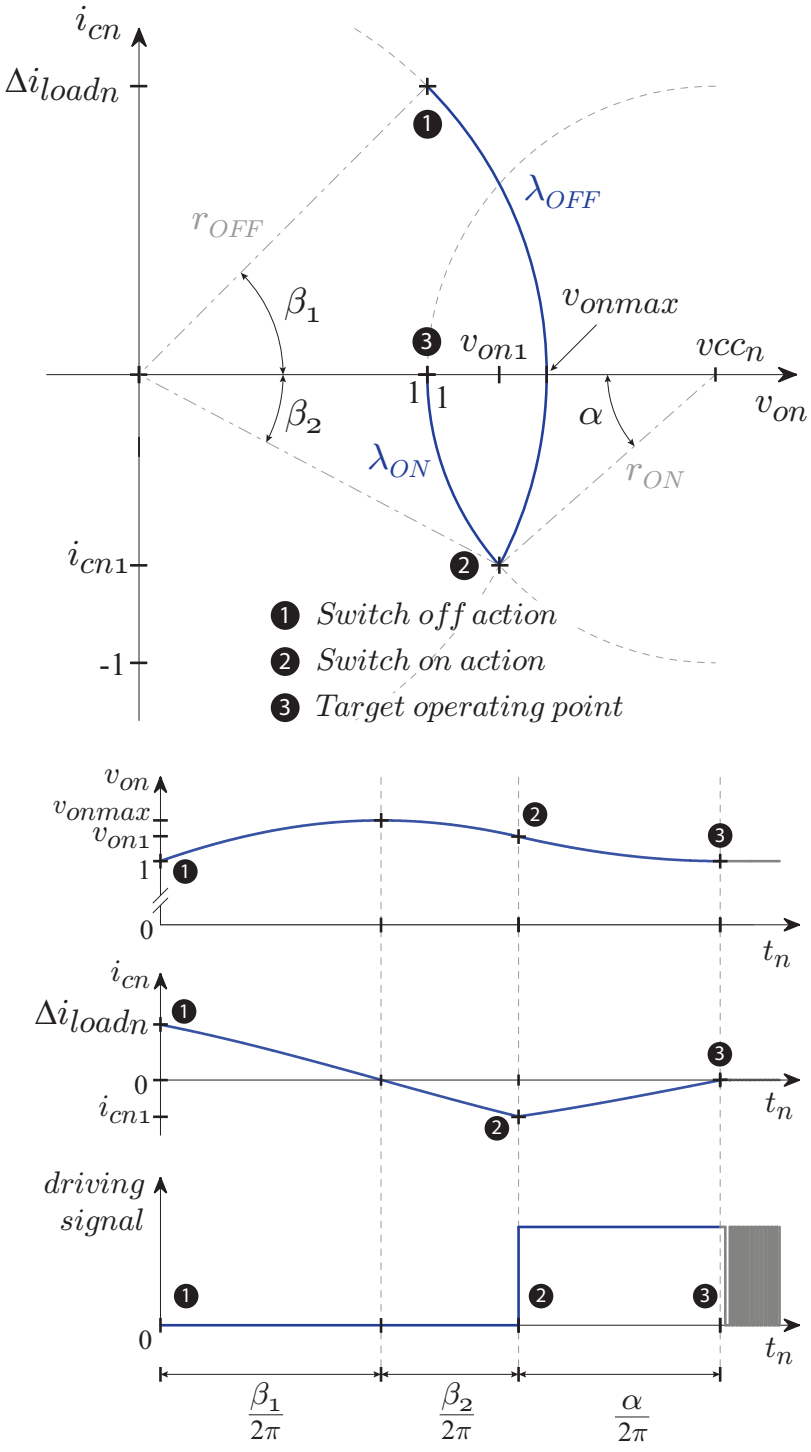

Figure 2.5: Unloading transient represented on geometrical and time domains.

2.3 Benchmarking Procedure Example

In this section, the start-up and loading transients of the $30W$ buck converter detailed in Table 2.1 are studied and compared with the theoretical physical limits.

Table 2.1: Buck converter parameters

PARAMETER	VALUE	NORM.
v_{ref}	12 V	1
V_{cc}	24 V	2
L	508 μH	$\frac{1}{2\pi}$
C	47.5 μF	$\frac{1}{2\pi}$

The compensation is performed using small-signal modeling and implementing the traditional lead technique. The closed loop response is shown in Fig. 2.6 for start-up and for a current step-up of 2.5A (no-load to full-load) transients.

The normalization parameters are $T_0 = 985\mu s$, $Z_0 = 3.25\Omega$, $v_{ref} = 12V$, and $i_{ref} = 3.7A$.

The ideal normalized start-up transient can be calculated using (2.10), (2.11), and (2.12) and depends only on the value of the normalized input voltage. For this case, where $V_{ccn} = 2$, the theoretical minimum settling time is $t_{startn} = 0.2902$. Denormalizing, the ideal start-up transient for the specified converter is obtained:

$$t_{start} = T_0 \; t_{startn} = 285\mu s \tag{2.24}$$

The settling time of the controller is $1.1ms$, which is 3.85 times the optimal. A clear opportunity for improvement is identified in the start-up transient.

In order to benchmark the response of the compensator during a current step-up transient, it is necessary to normalize the converter parameters. The normalized current step-up is given by:

$$\Delta i_{loadn} = \frac{\Delta iload}{i_{ref}} = 0.678 \tag{2.25}$$

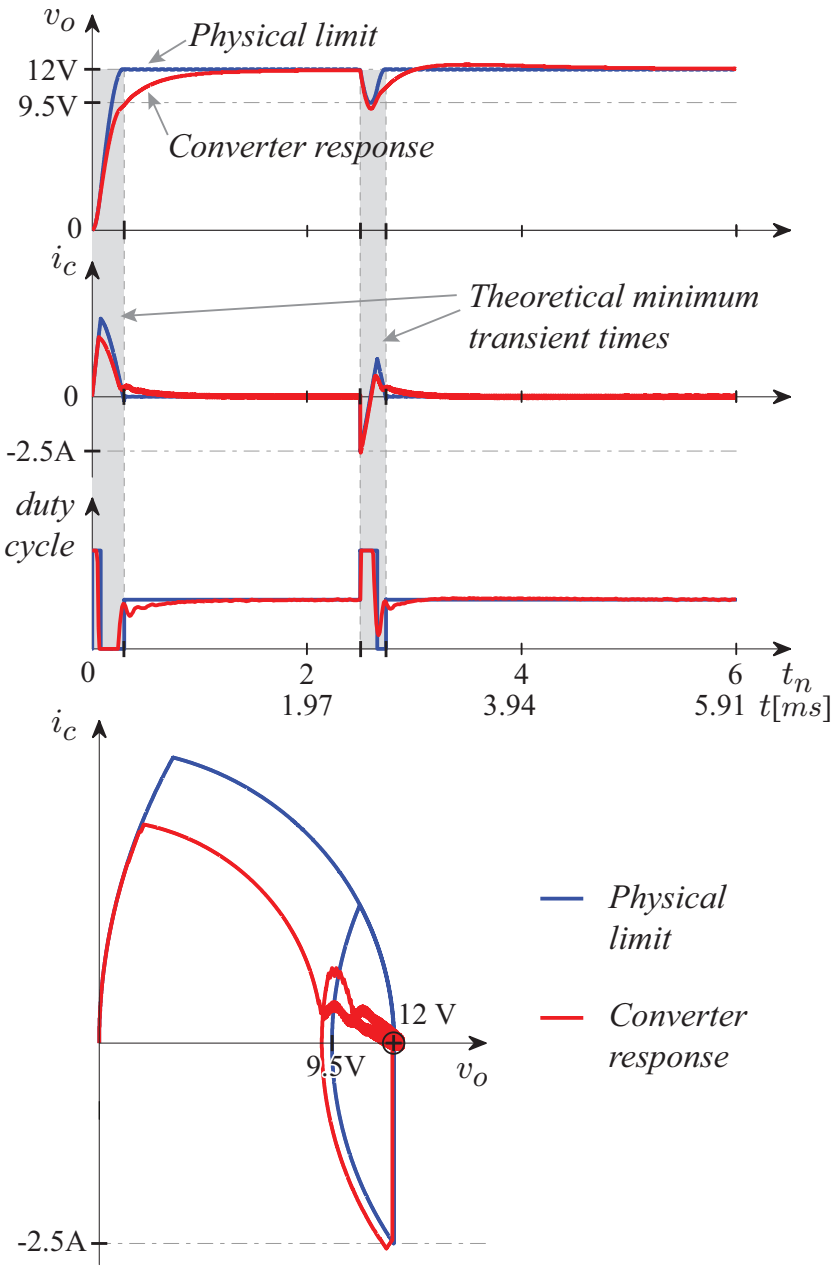

Figure 2.6: Comparison between physical limit operation and traditional compensation techniques.

Using (2.17) and (2.18), the normalized theoretical minimum recovery time and voltage drop for the transient under study are found as 0.235 and 0.208 respectively, denormalizing:

$$t_{rec(min),Loading} = 230\mu s \tag{2.26}$$

and,

$$\Delta v_{o(min)} = 2.5V \tag{2.27}$$

The characteristic parameters of the linear controller transient response are a recovery time of $1.35ms$ and a maximum drop of $2.95V$. The physical limit of operation is shown in Fig. 2.6 and compared with the response of linear compensator. In this way, the opportunities to improve the classical control technique can be objectively assessed.e the classical control technique can be objectively assessed.

2.4 Experimental Results

Experimental results of the converter operating at the physical limit are shown in geometrical and time domains in Figs. 2.7 and 2.8, where the main parameters have been indicated and compared with the theoretical values. The prototype filter values are $L = 512\mu H$ and $C = 48\mu F$, which leads to a natural period T_0 of $985\mu s$.

In Fig. 2.7 the start-up transients for two different normalized input voltages, $V_{ccn} = 1$ and $V_{ccn} = 10$, are shown and compared with the ideal minimum times. For $V_{ccn} = 1$ the measured start up time is $340\mu s$ while the theoretical minimum is $328\mu s$. For $V_{ccn} = 10$ the start up time is $262\mu s$, which approximates the quarter of T_0 ($246\mu s$) due to the high normalized input voltage.

Fig. 2.8 shows the three studied transient responses of the designed converter. The measured start up time is $290\mu s$, while the theoretical one for $V_{ccn} = 2$ can be obtained from (2.10) and is $285.65\mu s$. In the case of the loading transient, the design values for

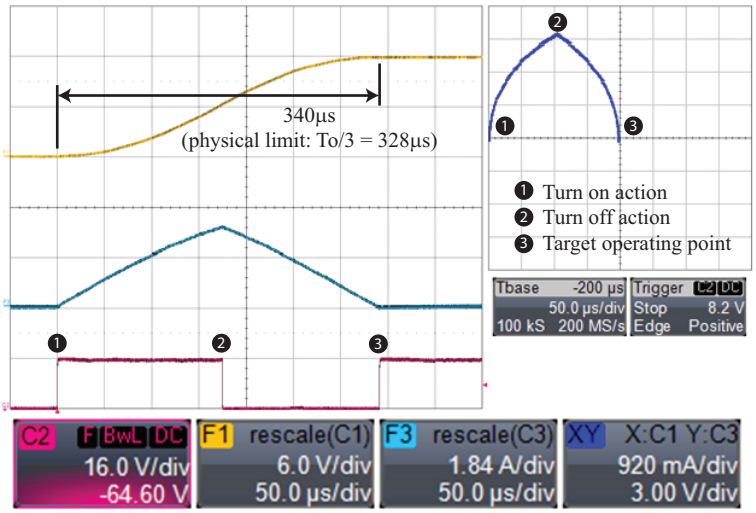

(a)

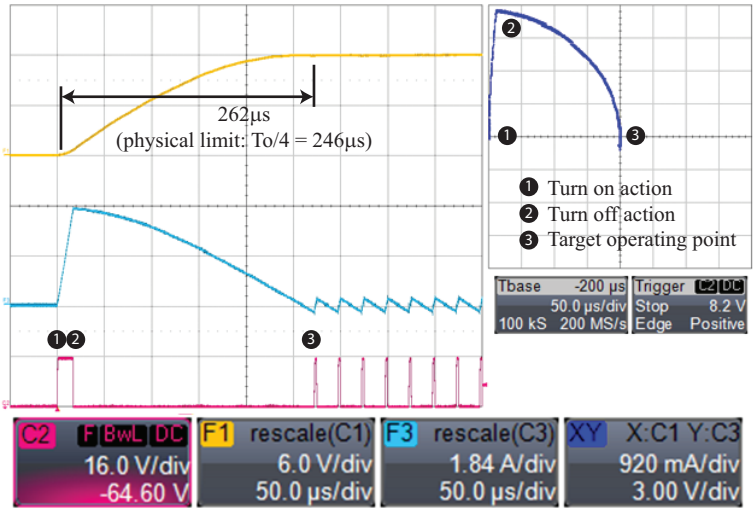

(b)

Figure 2.7: Start-up experimental results for a) low step-down ($V_{ccn} = 1$) and b) high step-down $V_{ccn} = 10$ transients.

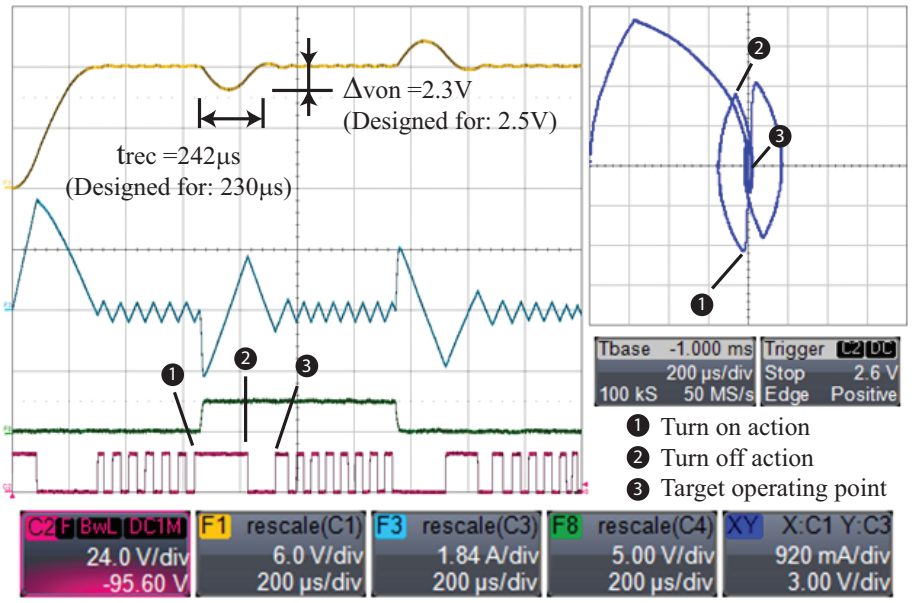

Figure 2.8: Start-up, loading and unloading transients for $V_{ccn} = 2$.

recovery time and voltage drop are is $230\mu s$ and $2.5V$, and the measured values are $242\mu s$ and $2.3V$ respectively. For the unloading transient, the theoretical values for recovery time and maximum voltage, calculated using (2.19) and (2.23), are $230\mu s$ and $14.5V$, while the measured values are $244\mu s$ and $14.7V$.

2.5 Summary

A detailed derivation of the theoretical physical limits of buck converters has been performed in this chapter. The theoretical optimal response for start-up, loading and unloading transients of buck converters have been fully characterized by general expressions obtained by geometrical analysis of the normalized converter.

Since the work is performed in the normalized domain, generality is gained and the expressions are valid for any possible filter values combination. The absolute minimum start up time for buck converters has been found, and the $T_0/4$ rule has been established.

A benchmarking tool was introduced by determining the absolute limits of performance, providing a practical tool for evaluating the behavior and comparing the performance of control strategies. A benchmarking procedure of a 30W, 24V/12V converter, based on transient response specifications, was performed and experimental results of the converter operating at physical limits were shown to validate the obtained mathematical expressions.

Chapter 3

Average Natural Trajectories (ANTs) for Buck Converters: Centric-Based Control

Many different control schemes have been developed for buck topologies in order to improve converter performance, achieve higher efficiency and reduce size and cost. In the previous chapter, a useful tool that enables the objective assessment of dynamic performance was introduced and, following a similar geometrical approach, a novel type of controller is developed here.

Linear techniques have been the preferred alternative since the 1970s [5, 6], while boundary techniques started gaining popularity in the late 1990s [47, 49]. These popular control schemes present advantages and disadvantages, inherent to the different natures of the approaches. For instance, a fixed frequency behaviour is obtained in linear techniques as a result of the averaged model employed, and a naturally bounded stable response is the result of the geometric-analysis performed in boundary techniques.

Combining the advantages of linear and boundary approaches, a new type of geometric-based controller is introduced in this chapter. The proposed scheme features fast and predictable behaviour as well as reliable operation during transients and in steady state. The cornerstone of the proposed controller is provided by a large-signal geometric-based model of the natural evolution of the averaged state variables, the Average Natural Trajectories

(ANTs). The ANTs of PWM driven buck converters are derived by merging traditional averaging techniques [5] and geometrical analysis. These trajectories are simple circles that represent the averaged paths the converter operating point follows for a given PWM duty cycle, providing an accurate model of the converter's large-signal behaviour.

Using the insight given by this model, the duty cycle necessary to achieve the target operating point can be calculated departing from any arbitrary initial condition. In contrast with boundary control techniques, where the control actions are ON/OFF, in the centric-based controller they are based on the definition of a PWM duty cycle. As a result, a new type of controller that narrows the gap between linear and boundary techniques is developed and referred to as centric-based control. Conceptual illustrations of the behaviour during start up of the centric-based, linear and sliding-mode controllers are detailed in Fig. 1.2. As indicated in the figure, the centric-based controller features shorter settling time than the linear and sliding-mode solutions, while the transient current peak is maintained at a lower value, which highlights the enhanced dynamic behaviour of the technique developed in this work. Fixed frequency operation (using PWM) and single duty-cycle transient solution are other characteristic features of the proposed controller depicted in the conceptual figure.

The defined trajectories are averaged over one PWM switching period, and therefore, fixed switching frequencies and low bandwidth requirements for sensing and signal conditioning systems are among the advantages of the proposed centric-based control. The computational burden of the proposed control technique is very low since, in an ideal case, calculations are performed just once to direct the operating point from an initial condition to the target operating point. The proposed normalized geometrical design framework provides the designer with not only generality, but also with an intuitive graphical representation of the behavior of the converter during transients. A detailed theoretical derivation to obtain the ANTs for buck converters is included in this work as well as the derivation of the control laws to implement the proposed technique. Experimental results of the target approaching principle

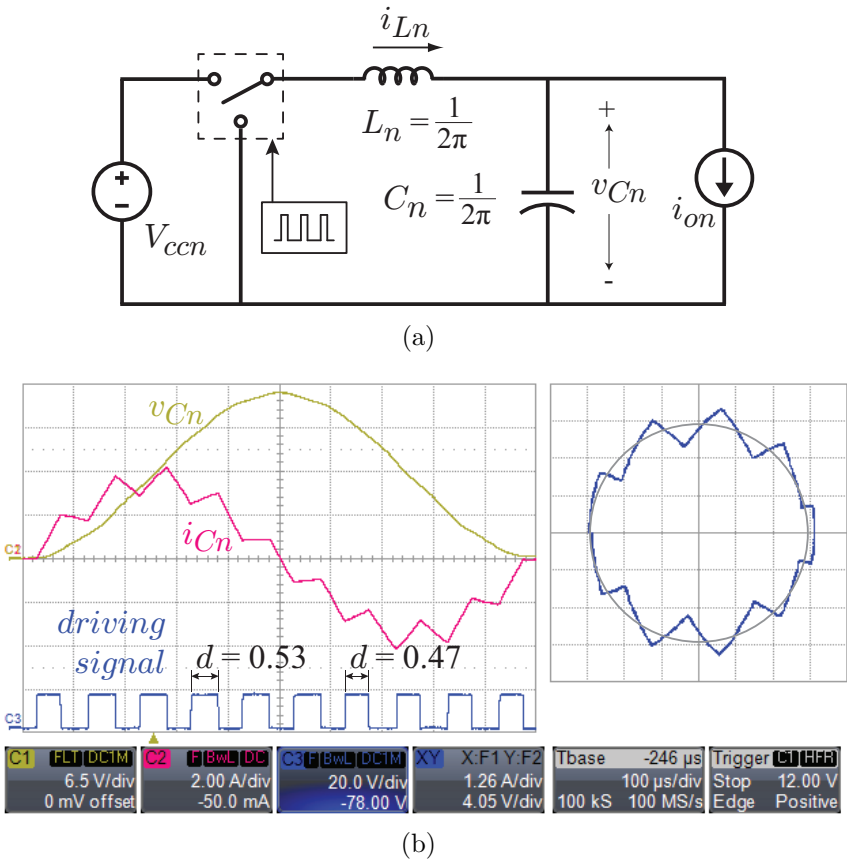

Figure 3.1: a) Normalized PWM driven buck converter. b) Pseudo-ideal natural trajectory forced in a real converter.

are shown in order to validate the obtained ANTs. Closed-loop results under different transients validate the enhanced performance of the proposed control scheme and highlight the practical usefulness of the concepts introduced in this chapter.

3.1 Buck Converter Ideal ANTs Derivation

The procedure to obtain the ANTs of the ideal PWM driven normalized buck converter shown in Fig. 3.2 is presented in this section. The effects of parasitic resistances are included later in this chapter.

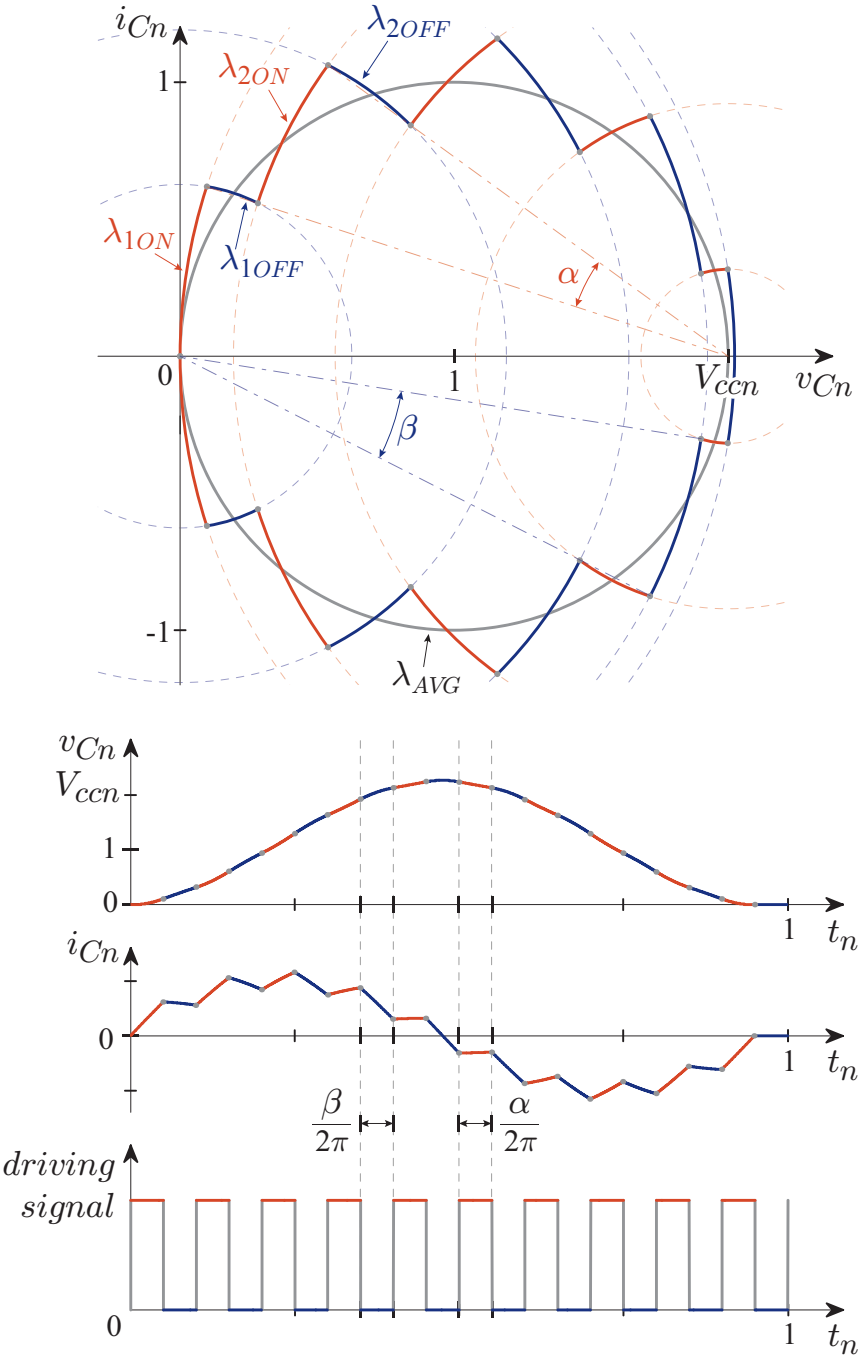

Figure 3.2: Ideal PWM natural trajectory with $V_{ccn} = 2$, $d = 0.5$ and $f_{sn} = 10$.

The differential equations that rule the behavior of buck converters are, for ON state:

$$C\frac{dv_C}{dt} = i_L - i_o \tag{3.1}$$

$$L\frac{di_L}{dt} = V_{cc} - v_C \tag{3.2}$$

and for OFF state:

$$C\frac{dv_C}{dt} = i_L - i_o \tag{3.3}$$

$$L\frac{di_L}{dt} = -v_C \tag{3.4}$$

In order to gain generality, the analysis is taken to the normalized domain, where:

$$t_n = \frac{t}{T_0}; \qquad Z_{xn} = \frac{Z_x}{Z_0}; \qquad v_{xn} = \frac{v_x}{v_{ref}}; \qquad i_{xn} = \frac{i_x}{i_{ref}}$$

and the employed base quantities are the filter characteristic impedance and resonance period, as well as the reference voltage and current:

$$Z_0 = \sqrt{L/C}\ ; \qquad T_0 = 2\pi\sqrt{LC}; \qquad v_{ref}\ ; \qquad i_{ref} = \frac{v_{ref}}{Z_0}$$

As a result, the normalized differential equations of the buck converter are found for ON,

$$\frac{1}{2\pi}\frac{dv_{Cn}}{dt_n} = i_{Ln} - i_{on} \tag{3.5}$$

$$\frac{1}{2\pi}\frac{di_{Ln}}{dt_n} = V_{ccn} - v_{Cn} \tag{3.6}$$

and OFF states.

$$\frac{1}{2\pi}\frac{dv_{Cn}}{dt_n} = i_{Ln} - i_{on} \tag{3.7}$$

$$\frac{1}{2\pi}\frac{di_{Ln}}{dt_n} = -v_{Cn} \tag{3.8}$$

The averaged differential equations describe the behavior of the converter when the normalized switching frequency ($f_{sn} = f_s\ T_0$) is much higher than the unity. Traditional averaging techniques are implemented to obtain the averaged differential equations in normalized form:

$$\frac{1}{2\pi}\frac{dv_{Cn}}{dt_n} = i_{Ln} - i_{on} \tag{3.9}$$

$$\frac{1}{2\pi}\frac{di_{Ln}}{dt_n} = d\ V_{ccn} - v_{Cn} \tag{3.10}$$

where d is the PWM duty cycle determined by the ratio between the ON time (T_{ON}) and the PWM period (T_s).

Solving the averaged differential equations the expressions that describe the time evolution of the averaged variables (capacitor voltage and inductor current) are found:

$$v_{Cn}(t_n) = [v_{Cn}(0) - d\ V_{ccn}]cos(2\pi t_n) + [i_{Ln}(0) - i_{on}]sin(2\pi t_n) + d\ V_{ccn} \tag{3.11}$$

$$i_{Ln}(t_n) = [i_{Ln}(0) - i_{on}]cos(2\pi t_n) + [v_{Cn}(0) - d\ V_{ccn}]sin(2\pi t_n) + i_{on} \tag{3.12}$$

By performing nodal analysis, the time domain expression of the capacitor current is determined:

$$i_{Cn}(t_n) = [i_{Ln}(0) - i_{on}]cos(2\pi t_n) - [v_{Cn}(0) - d\ V_{ccn}]sin(2\pi t_n) \tag{3.13}$$

Combining (3.11) and (3.13) the normalized time t_n is eliminated, yielding to the parametric representation of the Averaged Natural Trajectories (ANTs) for ideal buck converters:

$$\lambda_{AVG} : i_{Cn}^2 + (v_{Cn} - d\ V_{ccn})^2 = i_{Cn}^2(0) + (v_{Cn}(0) - d\ V_{ccn})^2 \tag{3.14}$$

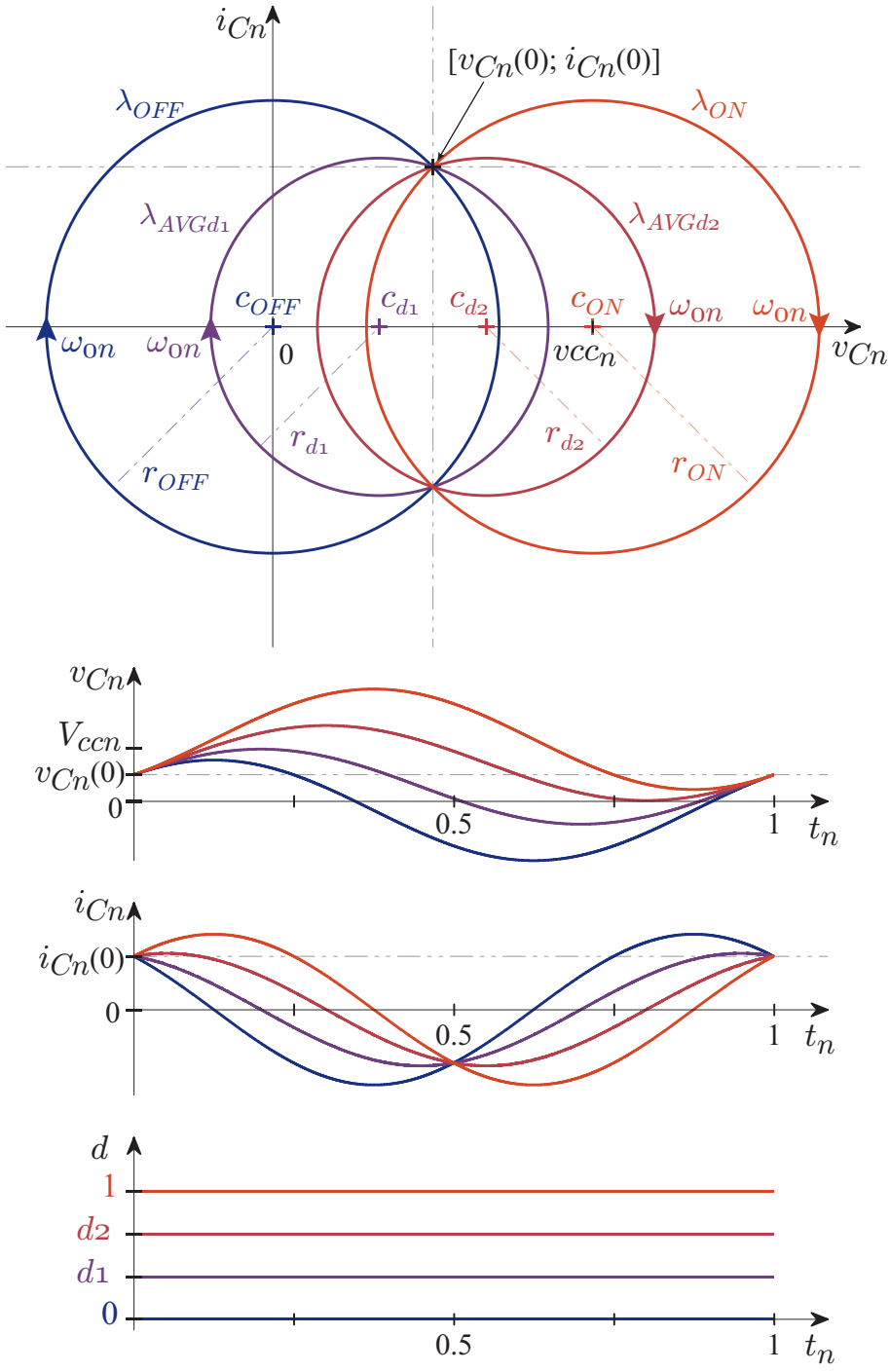

Figure 3.3: Several PWM-driven buck converter ANTs departing from unique initial operating point.

This equation represents the averaged trajectory that the operating point follows for any given duty cycle. It can be represented in the plane formed by v_{Cn} and i_{Cn} by a circle with center at $(d\ V_{ccn}; 0)$, and radius determined by the initial conditions $[v_{Cn}(0); i_{Cn}(0)]$. Fig. 3.3 shows the natural evolution of the averaged variables in both geometrical and time domains for several duty cycle values (centers).

PWM duty cycle values of $d_{OFF} = 0$, $d_1 = 0.33$, $d_2 = 0.67$, and $d_{ON} = 1$, illustrate the whole range of possible ANTs corresponding to an initial operating point $[v_{Cn}(0); i_{Cn}(0)]$.

The direct relationship between the circular trajectory center and the PWM duty cycle, given by $c = d\ V_{ccn}$, must be highlighted, due to the importance it represents for the control technique proposed in the following sections.

From (3.11) and (3.13), the normalized angular speed at which the averaged operating point moves across the circular path is constant and is given by $\omega_{on} = 2\pi$, as depicted in Figs. 3.1(b) (experimental) and 3.2 (simulation).

When the duty cycle saturates at either of its extremes given by $d = 1$ and $d = 0$, the converter follows the λ_{ON} and λ_{OFF} trajectories (shown in Fig. 3.3), which are referred to as natural trajectories rather than ANTs, since the switch is not in PWM mode for those cases. Equations (3.11), (3.13), and (3.14) are still valid for those cases, and since there are no switching actions involved, there is no average and the trajectories determine the actual natural trajectories of the converter.

It is also possible to find the real (non-averaged) paths that the operating point follows, shown in Fig. 3.2. The λ_{kON} and λ_{kOFF} trajectories are followed for $(k-1)T_{Sn} \leq T_n \leq (k-1+D)T_{Sn}$ and $(k-1+D)T_{Sn} \leq T_n \leq kT_{Sn}$ respectively, where k is the number of switching period, and the initial conditions of each subinterval are given by the final conditions of the previous state. Although the results would describe exactly the path followed, the advantages of working with the simplified averaged model would be lost and the complexity increased significantly.

3.2 Approaching the Target

As can be seen in Fig. 3.3, for any given initial conditions, there is a theoretically infinite number of averaged circular trajectories (in practice, the number is as high as the PWM resolution). One of those trajectories, and only one, is a circle that contains both initial and target points. For the ideal converter, the center of that circle can be found by performing a geometrical analysis from Fig. 3.4:

$$c_x = \frac{v_{Cn}(0)^2 + i_{Cn}(0)^2 - 1}{2\ (v_{Cn}(0) - 1)} \tag{3.15}$$

Since $c = d\ V_{ccn}$, then:

$$d_x = \frac{v_{Cn}(0)^2 + i_{Cn}(0)^2 - 1}{2\ V_{ccn}\ (v_{Cn}(0) - 1)} \tag{3.16}$$

Using this equation, the duty cycle needed to reach the target operating point following just one averaged circular path can be determined.

The time that it takes for the operating point to reach the target can be determined from Fig. 3.4 by finding the angle β_1 and dividing it by $\omega_{on} = 2\pi$. Using trigonometrical definitions, the transient time is found as,

$$t_D = \frac{1}{2\pi}\ cos^{-1}\left(\frac{v_{Cn}(0) - c}{1 - c}\right) \tag{3.17}$$

Once the target is reached, the center must be moved to the steady state operating point by setting the duty cycle to $\frac{1}{V_{ccn}}$, in order to obtain an averaged circular trajectory with null radius.

In theory, and for infinite switching frequency, the operating point remains at the target without moving. However, in practice and for limited switching frequencies, the operating point becomes an operating path determined by λ_{ON} and λ_{OFF} trajectories, which define voltage and current ripples.

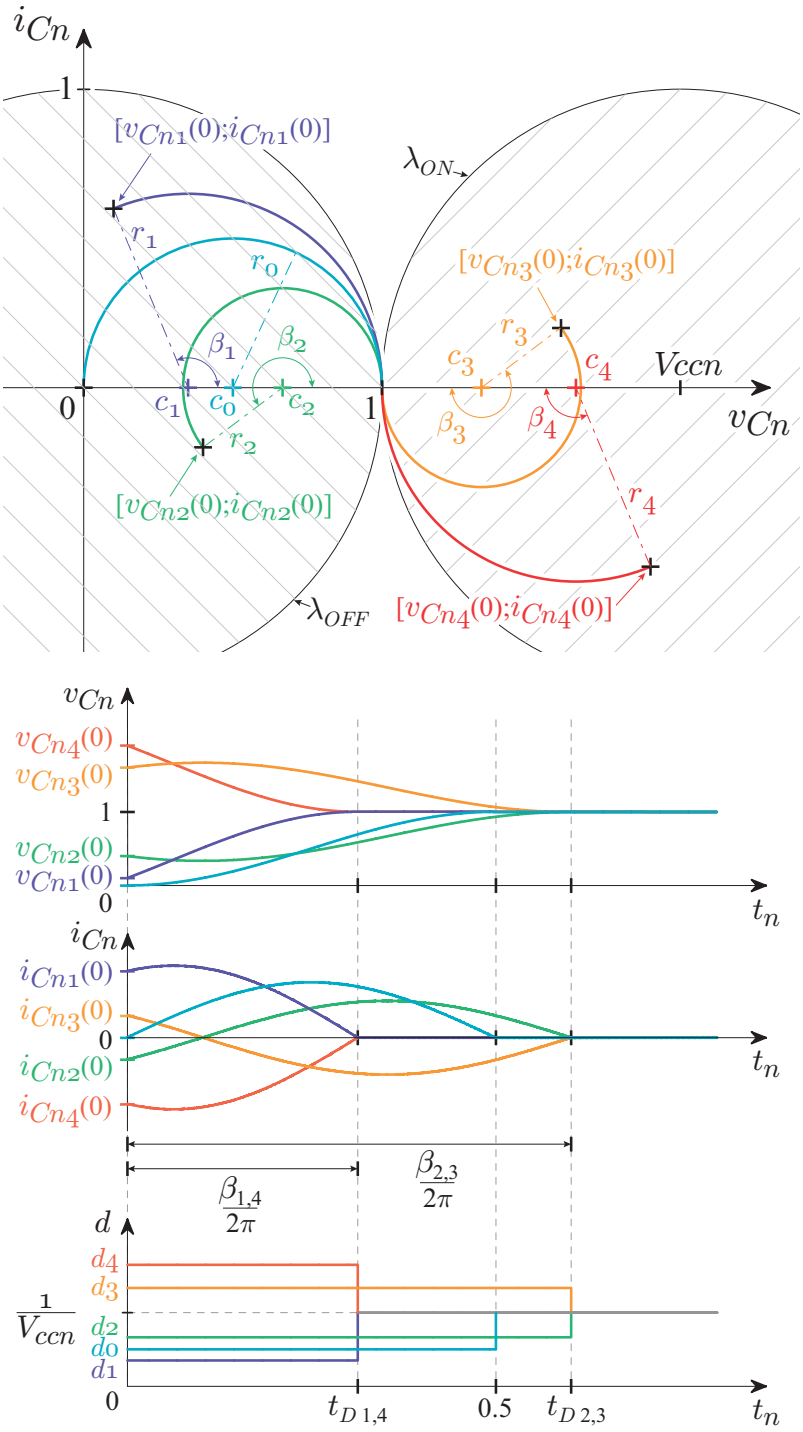

Figure 3.4: Ideal fixed duty cycle target approaching method for different initial conditions

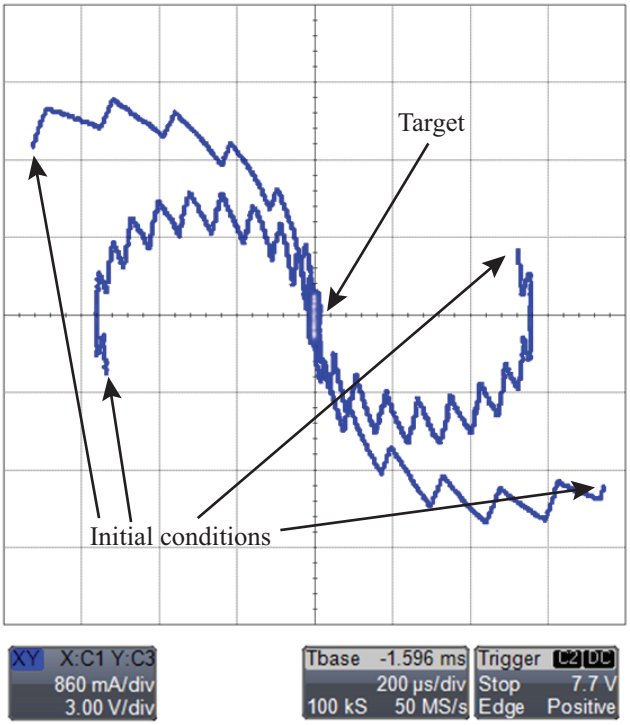

Figure 3.5: Fixed duty cycle target approaching method forced in a real converter

The result of the analysis reveal a simple and powerful concept: the target operating point can be reached following only one ANT by setting a duty cycle corresponding to a determined center location which depends only on the initial operating point location.

3.3 Closing the Loop with a Centric-Based Controller

A new geometric-based, fixed-frequency control technique based on (3.15) is presented in this section. Fig. 3.6 (a) shows a block diagram of the proposed controller, and Fig. 3.6 (b) shows the results of the implementation in an experimental setup.

The control scheme is composed of three main principles. A periodic center recalculation using (3.15) defines the main control law, which is complemented with extra restrictions to the function domain to improve dynamic response and a linear term to eliminate possible steady state error. The three principles are described in the following subsections.

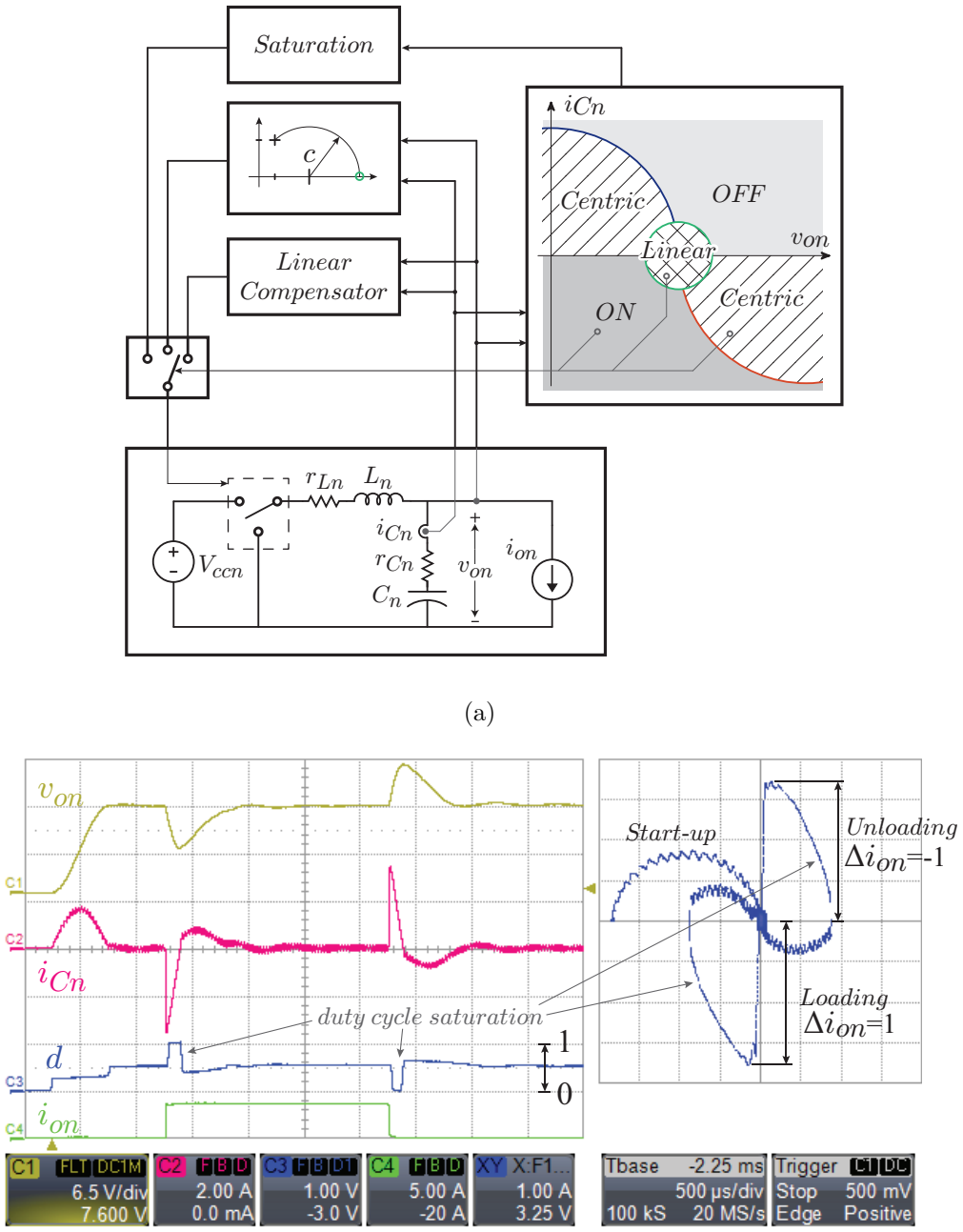

Figure 3.6: Centric-based controller: a) scheme, and b) experimental results.

3.3.1 Periodic Center Calculation

Using (3.15), the center of the circle that directs the operating point to the target is calculated based only on the location of the averaged operating point. Tolerances in the values of reactive components, as well as losses present in the system, can cause the converter's averaged behaviour to differ from the ideal circular trajectories derived. Performing a periodical center recalculation using updated values of the averaged capacitor current and voltage as initial conditions, these deviations are limited to the magnitude they reach over one recalculation period.

3.3.2 Domain Restrictions

The domain of the control law equation (3.15) is determined by the saturation trajectories λ_{ON} and λ_{OFF} shown in Fig. 3.4. Otherwise, the converter's operating point must be taken back into the function domain by setting the duty cycle to one of its extremes before attempting to perform the center calculation. Extra restrictions are applied to the function domain in order to improve the converter dynamic behaviour as shown in Fig. 3.6(a). The restricted domain is defined as the positive capacitor current half of λ_{OFF} and negative capacitor current half of λ_{ON}. In this way, since saturation trajectories are followed right after load transients, the magnitude of drops and spikes in the output voltage are minimized, reaching near-optimal values.

3.3.3 Steady State Error Correction

Effects not being considered in the model can also affect the steady state behaviour, leading to undesired steady state error. For instance, the duty cycle needed in a buck converter with $V_{ccn} = 2$ working at full load might be 0.51 instead of $\frac{1}{V_{ccn}} = 0.5$. Even when this effect might be minimal in high-efficiency converters, it is worth addressing it in order to

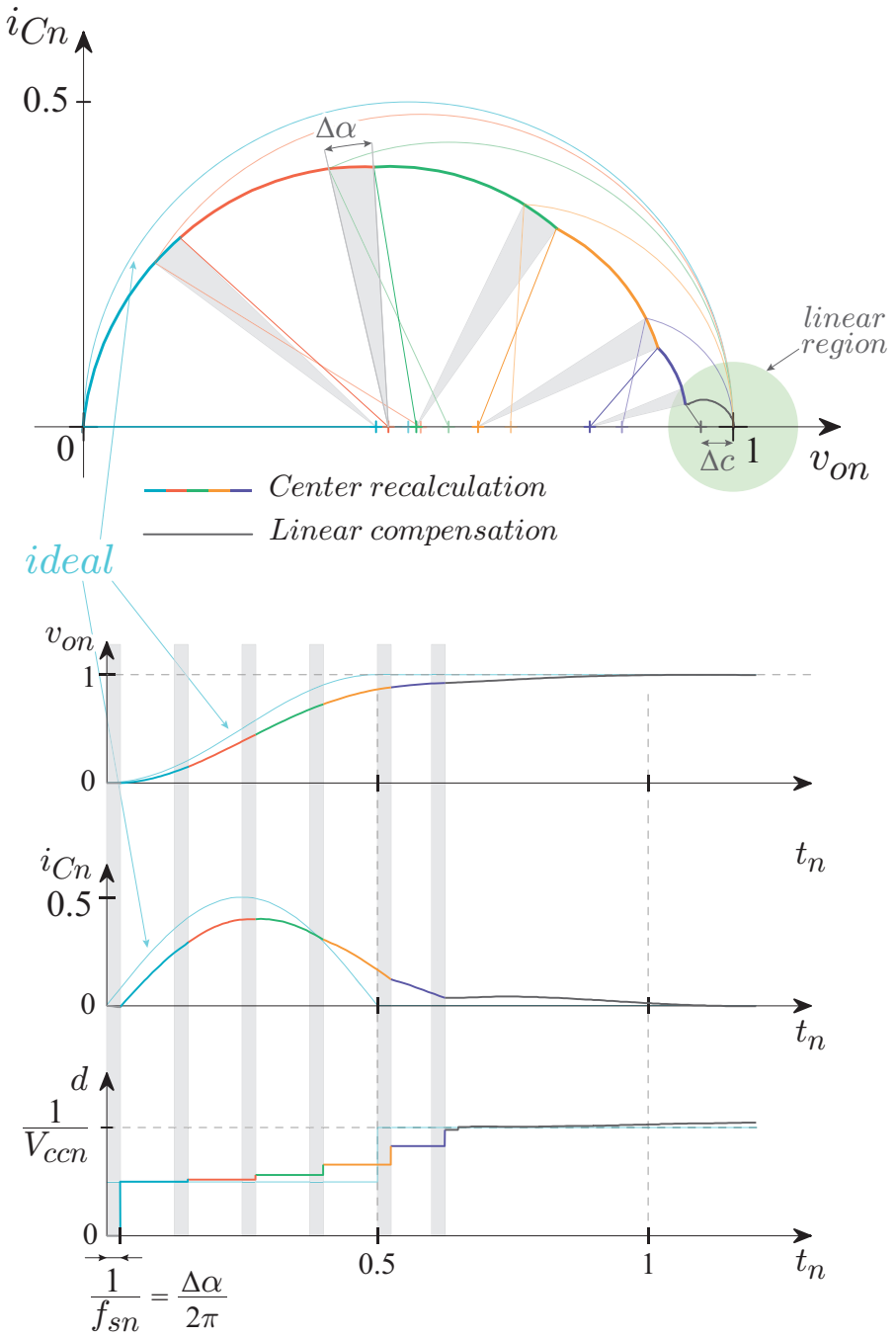

Figure 3.7: Closed-loop controller concept

present a complete solution. The approach proposed here is based on the implementation of a linear controller that is engaged once the operating point reaches the target neighborhood, as indicated in the scheme of Fig. 3.6 (a).

In this way, when the operating point is close enough to the target, the duty cycle is set to the ideal value ($\frac{1}{V_{ccn}}$) plus the output of a linear term. Implementing a dual-loop compensator using output voltage and capacitor current becomes an appealing option for this purpose since the variables are already being measured.

A conceptual illustration of the behaviour of the complete controller is provided in Fig. 3.7 for a start-up transient. The differences between the ideal trajectories and the obtained ones, as well as the effect of the center recalculation, can be observed during the initial part of the transient. When the indicated target neighborhood area is reached, the linear term is engaged, and the steady state error is eliminated. It is also worthwhile to observe the $\frac{1}{f_{sn}}$ delay introduced to the control action, which is produced by the fixed-frequency nature of the approach.

3.4 Experimental Results

Experimental results that validate the theoretical concepts and the presented control technique have been obtained using the $44W$ buck converter detailed in Tables 3.1 and 3.2.

The experimental capture of 3.1(b) illustrates pseudo-ideal ANTs obtained from a real converter operating at a normalized switching frequency $f_{sn} = 10$. In Fig. 3.5, the fixed duty cycle target approach method is shown for four different initial conditions with $f_{sn} = 20$.

Experimental results of the proposed closed-loop method are shown in Fig. 3.6(b), showing a fast and predictable response during start-up and extreme loading/unloading transients ($\Delta i_{on} = 1$). Small oscillations are observed when the operating point enters the target neigh-

Table 3.1: Buck converter parameters

PARAMETER	VALUE	NORM.
v_{ref}	12 V	1
V_{cc}	24 V	2
L	508 μH	$\frac{1}{2\pi}$
C	47.5 μF	$\frac{1}{2\pi}$
T_0	985 μs	1
Z_0	3.25 Ω	1

Table 3.2: Main parasitics

PARAMETER	VALUE	NORM.
r_L	180 $m\Omega$	$33.4m$
r_C	71 $m\Omega$	$21.8m$
$r_{switch1}$	20 $m\Omega$	$6.15m$
$r_{switch2}$	20 $m\Omega$	$6.15m$

borhood area. Due to the effect of losses, when the step in the duty cycle is produced, the center is not located exactly at the target, causing a non-null averaged trajectory which translates into small oscillations. The linear term is engaged at the same moment and leads the operating point to finally reach the target.

Further experimental results of the proposed centric-based controller are shown in the following sections, which compare the technique with classical linear schemes and analyze the sensitivity to changes of the value of reactive components. The saturation of the duty cycle for operating points not contained in the restricted domain, as well as the centric controlled trajectories, can be noticed in all the centric-based controller experimental captures.

3.5 Comparison with Linear Controllers

The control technique presented here shows a fast and predictable response for large transients such as start-up and high step loading/unloading. In this section, experimental results of a centric-controlled buck converter are compared with the ones obtained using a classical dual-loop linear compensator in order to benchmark the performance of the proposed scheme.

The performances of both controllers under the same transient conditions are presented in Figs. 3.8, 3.9, and 3.10. The main normalized transient characteristics (normalized transient time, voltage and current peak deviations) have been indicated in the figure and are

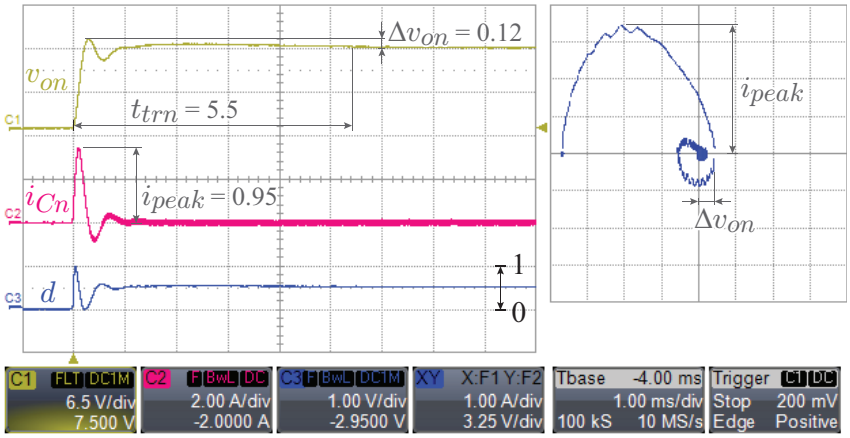

(a)

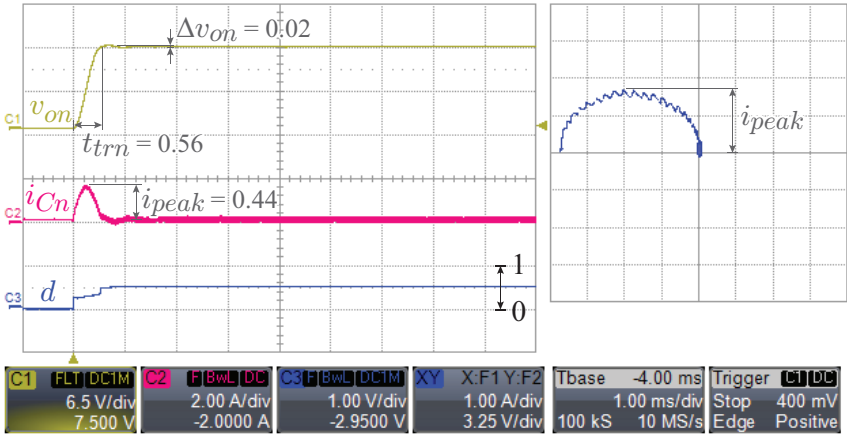

(b)

Figure 3.8: Comparison between dual-loop linear and centric-based controllers. Start-up transient for a) linear, and b) centric-based.

summarized in Table 3.3 in order to facilitate an objective assessment.

The steady state region employed to measure transient recovery times is defined as ±2% of the reference voltage.

Start-up transients are shown in Fig. 3.8 for linear and centric-based controllers respectively. In the case of the linear controller, steady state is reached after 5.5 resonance periods T_0 ($5.4ms$) with a voltage overshoot of 12% ($1.44V$) and a normalized current peak of 0.95 ($3.5A$). The proposed controller exhibits a settling time almost ten times faster (0.56 T_0 or $0.55ms$) with a normalized current peak of 0.44 ($1.63A$) and almost no overshoot (0.02 v_{ref}).

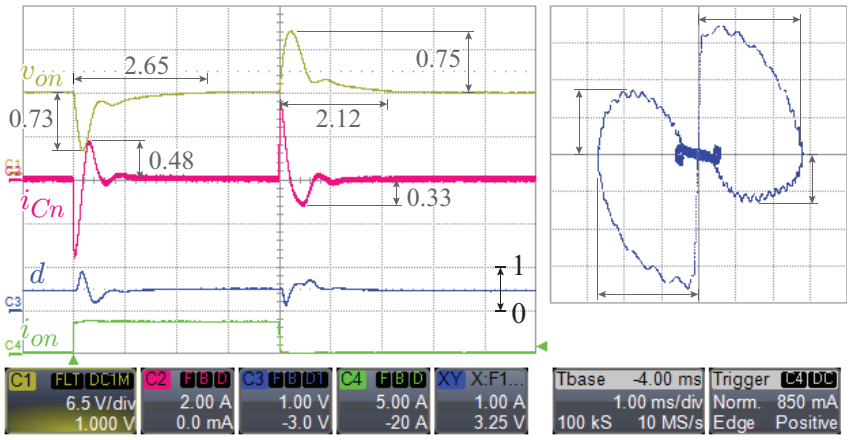

(a)

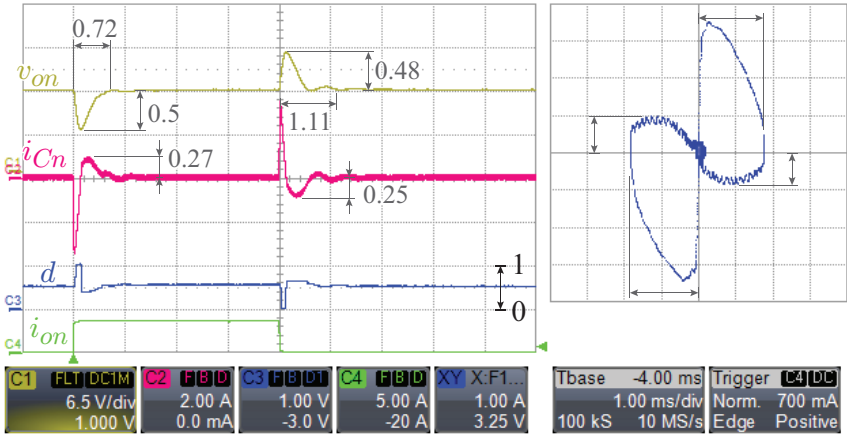

(b)

Figure 3.9: Comparison between dual-loop linear and centric-based controllers. Loading/unloading transients with $\Delta i_{on} = 1$ for a) linear, and b) centric-based.

Table 3.3: Centric - linear controllers comparison

TRANSIENT		t_{trn}		Δv_{on}		i_{peak}	
	Δi_{on}	Lin.	Cen.	Lin.	Cen.	Lin.	Cen.
Start-up		5.5	0.56	0.12	0.02	0.95	0.44
Loading	1	2.65	0.72	0.73	0.5	0.48	0.27
	0.5	1.88	1	0.35	0.19	0.25	0.12
Unloading	1	2.12	1.11	0.75	0.48	0.33	0.25
	0.5	1.78	1.1	0.36	0.18	0.22	0.1

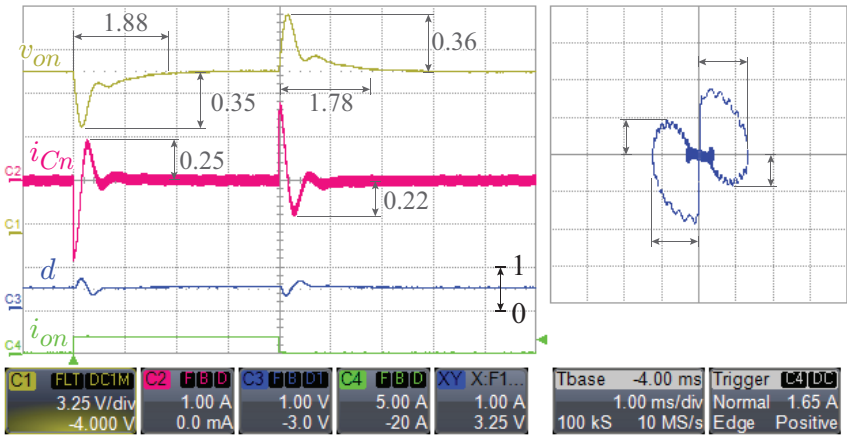

(a)

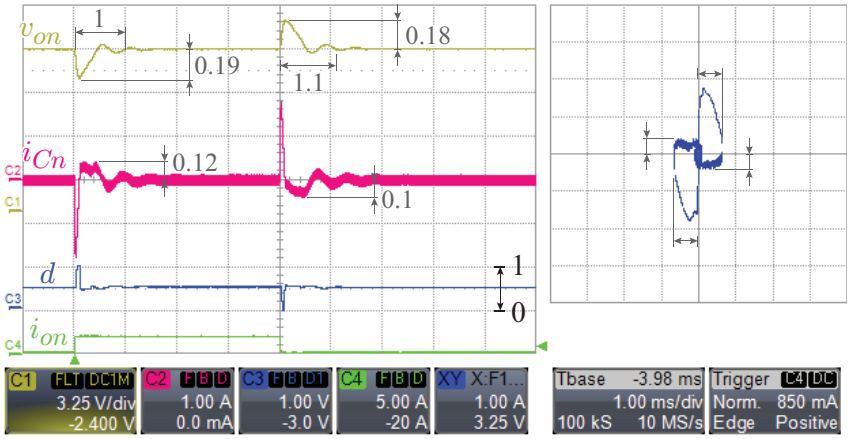

(b)

Figure 3.10: Comparison between dual-loop linear and centric-based controllers. Loading/unloading transients with $\Delta i_{on} = 0.5$ for a) linear, and b) centric-based.

Regarding the geometrical-domain plots, it is worth highlighting the predictable behavior featured by the centric controller.

The responses of the controllers to unity normalized magnitude current step-up and step-down transients ($3.7A$ - extremely large transient) are shown in Fig. 3.9. The normalized recovery times presented by the linear-controlled converter are 2.65 ($2.61ms$) for step-up transient and 2.12 ($2.08ms$) for step-down transient. In the centric-based controller implementation, these times are reduced to 0.72 ($0.71ms$) and 1.11 ($1.09ms$) respectively.

The normalized voltage drops and peaks during the transients are also smaller in the centric-based case, featuring 0.5 ($6V$) and 0.48 ($5.76V$) against the 0.73 ($8.76V$) and 0.75 ($9V$) presented in the linear case. Following the same trend, the current peaks are reduced from the values 0.48 ($1.77A$) and 0.33 ($1.22A$) they present in the linear case, to 0.27 ($1A$) and 0.25 ($0.93A$) for the centric controller. In the geometrical domain, the large transient response of the centric-based controller is, once more, proven to be very predictable. Small unpredicted behaviours are shown in the target neighborhood due to the center misplacement issue, which is addressed in previous sections and solved by a complementary linear compensator.

One more performance comparison between the controllers is shown in Fig. 3.10; in this case the current step-up and down magnitude is one half of the reference current ($1.85A$). For this transient, half of the centric-based controller recovery time is determined by the complementary linear term. For this reason, the difference between the controllers performance is reduced, as detailed in Table 3.3. Even in this case, the performance of the centric controller is still 60% faster than the traditional dual-loop linear controller (at worst), while the voltage and current deviation peaks are still 50% lower.

3.6 Tolerances Sensitivity Analysis

The converter ANTs are strongly related to the values of the main reactive components in the circuit and their tolerances. Therefore, and in order to illustrate how well the proposed control technique behaves under variations of these parameters, experimental results including $\pm 20\%$ deviations in the component values are shown in Figs. 3.11 and 3.12. The deviations in the component values cause the system characteristic impedance Z_0 and natural resonance time T_0 to differ from the values used in the normalization, producing distortions in the expected behaviour. The resulting characteristic parameters and responses are shown in Table 3.4 for each one of the cases under analysis.

(a)

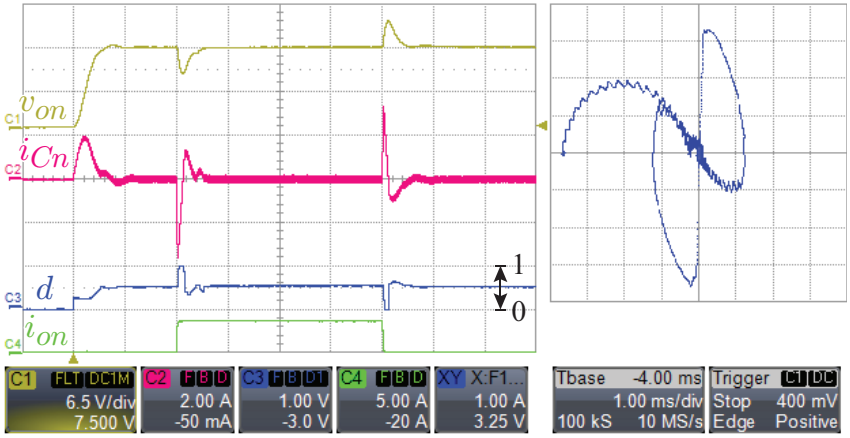

(b)

Figure 3.11: Centric-based controller performance under parameter deviations. Start-up, loading and unloading transients for a) $L_{real} = 0.8\ L$, $C_{real} = 0.8\ C$; and b) $L_{real} = 0.8\ L$, $C_{real} = 1.2\ C$;

Table 3.4: Centric controller parameter deviations

	Parameter deviation				Loading transient response		
Fig.	L	C	Z_0	T_0	t_{recn}	Δv_{on}	i_{peak}
3.11 (a)	−20%	−20%	0	−20%	+19%	+4%	−11%
3.11 (b)	−20%	+20%	−18%	−2%	−19%	−36%	+30%
3.12 (a)	+20%	−20%	+22%	−2%	+33%	+24%	−15%
3.12 (b)	+20%	+20%	0	+20%	+22%	−3%	−20%

(a)

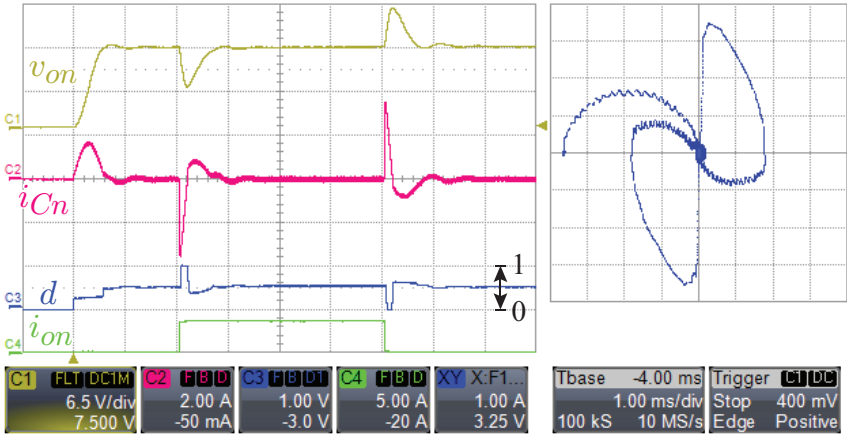

(b)

Figure 3.12: Centric-based controller performance under parameter deviations. Start-up, loading and unloading transients for a) $L_{real} = 1.2\ L$, $C_{real} = 0.8\ C$; and b) $L_{real} = 1.2\ L$, $C_{real} = 1.2\ C$.

The deviations in resonance period and characteristic impedance can be observed in both time and geometrical domain plots. Comparing the time domain plots of Figs. 3.11 (a) and 3.12 (b), the variations in T_0 become evident when it is observed how the recovery time in the first one is shorter than in the second one. The effects of changes in Z_0 are evident in the geometrical domain plots of Fig. 3.11 (b) and 3.12 (a), in which the circular trajectories are distorted. As proven by the experimental results in shown Figs. 3.11 (a) and 3.12 (b), the proposed control scheme behaves reliably under large variations in the system parameters.

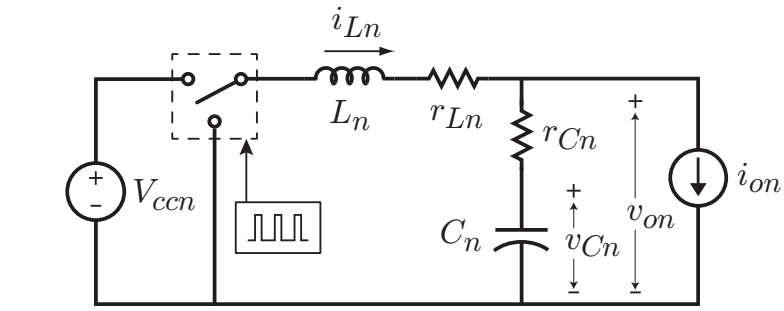

(a)

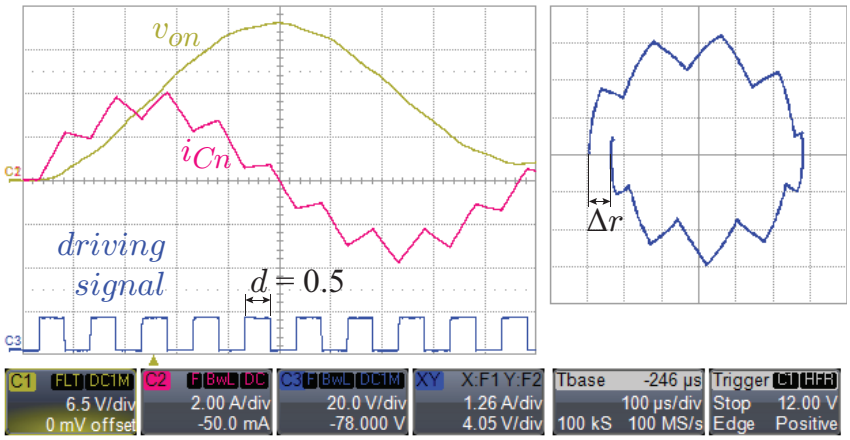

(b)

Figure 3.13: a) Non-ideal normalized PWM driven buck converter. b) Real PWM natural trajectory.

Fast responses are obtained and the predictability of the trajectories is kept within acceptable margins even for large parameter deviations.

3.7 Buck Converter Non-Ideal ANTs Derivation

The ANTs of the non-ideal normalized buck converter shown in Fig. 3.13, including normalized parasitic resistances in the inductor and capacitor (r_{Ln} and r_{Cn} respectively) are derived in this section. The insight provided here features important conceptual value and enables the derivation of a closed-loop centric-based controller without the need of a linear component to solve steady state issues.

The differential equations that represent the normalized converter are:

$$\frac{1}{2\pi}\frac{dv_{Cn}}{dt_n} = i_{Ln} - i_{on} \tag{3.18}$$

$$\frac{1}{2\pi}\frac{di_{Ln}}{dt_n} = d\ V_{ccn} - i_{Ln}\ r_{Ln} - i_{Cn}\ r_{Cn} - v_{Cn} \tag{3.19}$$

Rearranging terms, (3.19) can be expressed as:

$$\frac{1}{2\pi}\frac{di_{Ln}}{dt_n} = d\ V_{ccn} - i_{on}\ r_{Ln} - i_{Cn}\ \ (r_{Cn} + r_{Ln}) - v_{Cn} \tag{3.20}$$

By solving the differential equations system formed by (3.18) and (3.20) time domain expressions that describe the time evolution of the state variables are identified as:

$$\begin{aligned} v_{Cn}(t_n) = Att(t_n)\ \Big\{&(v_{Cn}(0) - c')\ cos(\omega_{dn}t_n) \\ &+ \left[(v_{Cn}(0) - c')\ \frac{r_{Cn} + r_{Ln}}{2} + (i_{Ln}(0) - i_{on})\right]\ \frac{\omega_{on}}{\omega_{dn}}\ sin(\omega_{dn}t_n)\Big\} + c' \end{aligned} \tag{3.21}$$

$$\begin{aligned} i_{Ln}(t_n) = Att(t_n)\ \Big\{&(i_{Ln}(0) - i_{on})\ cos(\omega_{dn}t_n) \\ &- \left[(i_{Ln}(0) - i_{on})\ \frac{r_{Cn} + r_{Ln}}{2} + (v_{Cn}(0) - c')\right]\ \frac{\omega_{on}}{\omega_{dn}}\ sin(\omega_{dn}t_n)\Big\} + i_{on} \end{aligned} \tag{3.22}$$

with:

$$\omega_{on} = 2\pi; \tag{3.23}$$

$$\omega_{dn} = \omega_{on}\ \sqrt{1 - \left(\frac{r_{Cn} + r_{Ln}}{2}\right)^2} \tag{3.24}$$

$$Att(t_n) = e^{-\omega_{on}t_n\sqrt{1-\left(\frac{\omega_{dn}}{\omega_{on}}\right)^2}} \tag{3.25}$$

$$c' = d\ V_{ccn} - i_{on}\ r_{Ln} \tag{3.26}$$

Where ω_{on} and ω_{dn} are the ideal and damped normalized resonance frequencies respectively. The time-dependent function $Att(tn)$ describes the attenuation of the radius along

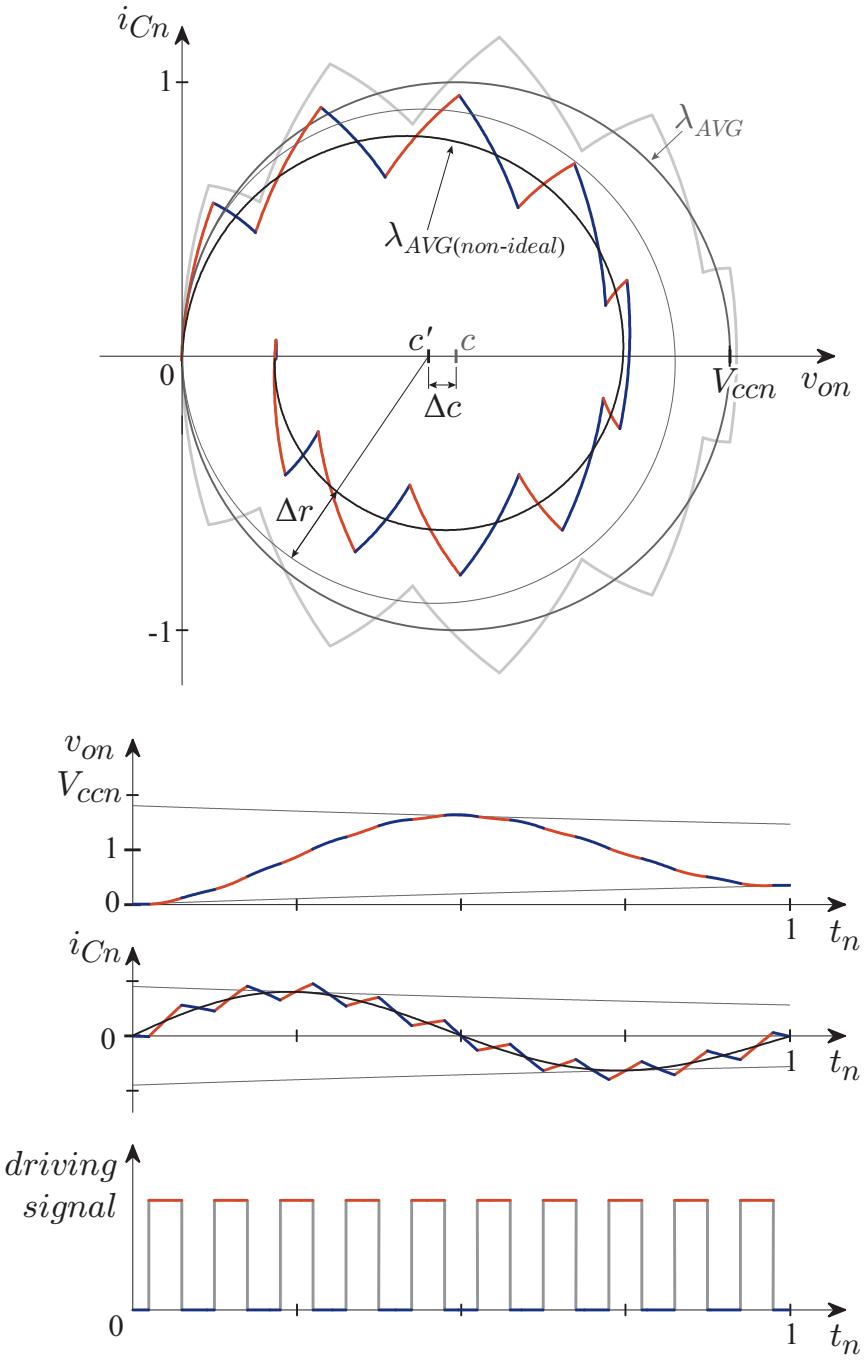

Figure 3.14: Non-ideal natural trajectory with $V_{ccn} = 2$, $d = 0.5$ and $f_{sn} = 10$.

the normalized time, and c' gives the location of the new center.

As in the lossless case, the capacitor current is given by:

$$i_{Cn} = i_{Ln} - i_{on} \tag{3.27}$$

Then, the time domain expression that describes it can be derived from (3.22) as:

$$i_{Cn}(t_n) = Att(t_n) \left\{ i_{Cn}(0)\ cos(\omega_{dn} t_n) - \left[i_{Cn}(0)\ \frac{r_{Cn} - r_{Ln}}{2} + (v_{on}(0) - c') \right] \frac{\omega_{on}}{\omega_{dn}}\ sin(\omega_{dn} t_n) \right\} \tag{3.28}$$

Since the capacitor equivalent series resistance is different than zero, the output voltage v_{on} is now determined by the addition of capacitor voltage and the drop on its ESR:

$$v_{on} = v_{Cn} + i_{Cn}\ r_{Cn} \tag{3.29}$$

Replacing (3.21) and (3.28) in (3.29), the time domain describing equation of the output voltage is found:

$$v_{on}(t_n) = Att(t_n) \left\{ (v_{on}(0) - c')\ cos(\omega_{dn} t_n) + \left[(v_{on}(0) - c') + i_{Cn}(0)\ (1 - r_{Ln}\ r_{Cn}) \right] \frac{\omega_{on}}{\omega_{dn}}\ sin(\omega_{dn} t_n) \right\} + c' \tag{3.30}$$

Combining (3.30) and (3.28) an implicit expression that describes the ANTs in non-ideal converters is found:

$$\lambda_{AVG(non-ideal)} : (v_{on} - c')^2 + (1 - r_{Ln}\ r_{Cn})\ i_{Cn}^2 + (r_{Ln} - r_{Cn})(v_{on} - c') i_{Cn} = r(0)\ Att(t_n) \tag{3.31}$$

where:

$$r(0) = (v_{on}(0) - c')^2 + (1 - r_{Ln}\ r_{Cn})\ i_{Cn}(0)^2 - (r_{Ln} - r_{Cn})\ (v_{on}(0) - c')\ i_{Cn}(0) \qquad (3.32)$$

Which represents a spiral given by an ellipse with initial radius $r(0)$ which exponentially decreases with the normalized time following the function $Att(t_n)$.

Fig. 3.14 shows the non-ideal ANTs for a normalized buck converter with normalized input voltage $V_{ccn} = 2$, switching frequency $f_{sn} = 10$, duty cycle $d = 0.5$, and series parasitic resistances $r_{Cn} = r_{Ln} = 0.1$.

The analysis performed in this section reveals differences between the particular case, when $r_{Cn} = r_{Ln} = 0$, and the general one; these differences can be summarized in three main points:

- The circle becomes a rotated ellipse
- The radii are attenuated by the function $Att(tn)$
- The center is shifted to the left by $\Delta c = i_{on}\ r_{Ln}$

Taking these differences into account, a purely-geometrical alternative is proposed in the following section.

3.8 Closed-Loop Controller Including Estimation of Parasitics

As found in the previous section and shown in Fig. 3.14, the ANTs centers are shifted to the left in non-ideal converters. The insight provided is used in this section to develop a purely geometrical alternative with no steady state error and with an absolutely predictable transient response.

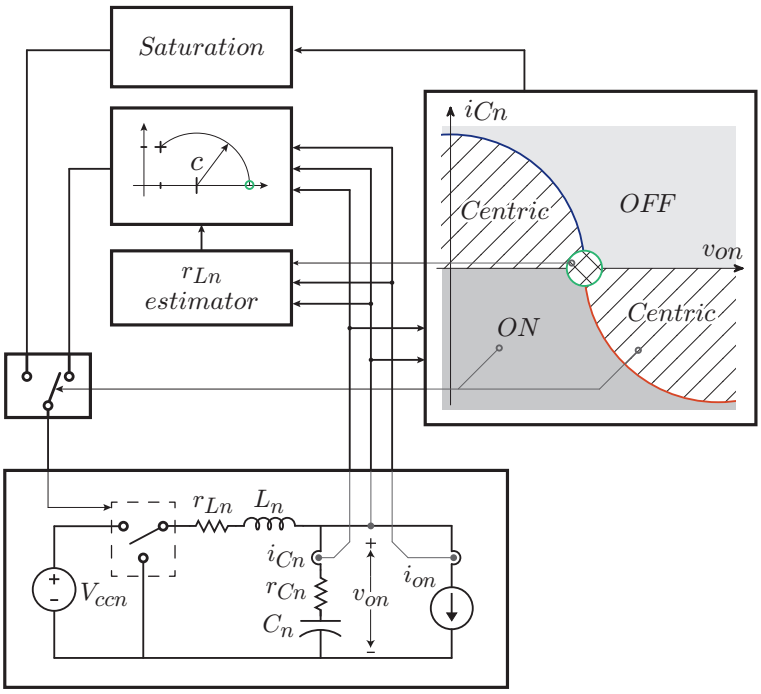

(a)

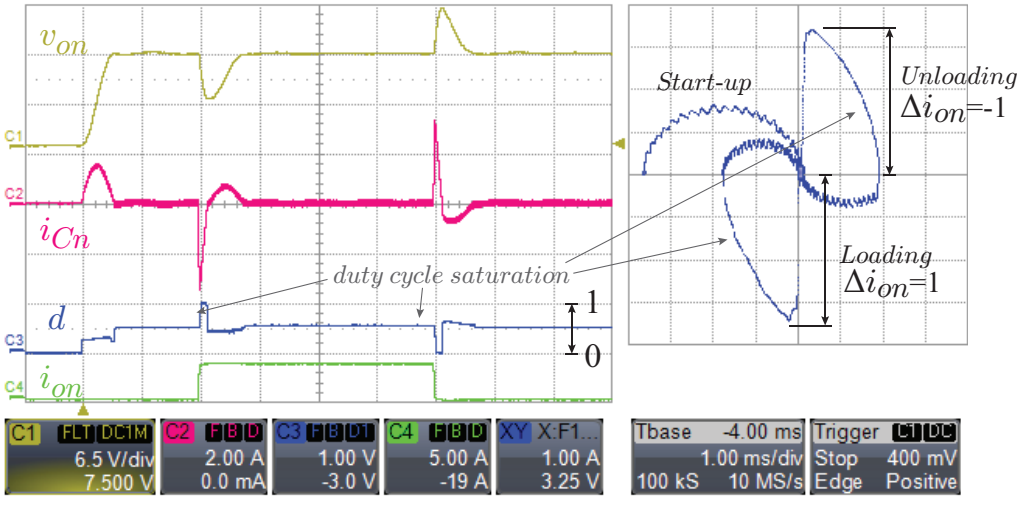

(b)

Figure 3.15: Centric-based controller with load current estimation: a) scheme, and b) experimental results.

From (3.26), the relation between duty cycle and ANTs center is given by:

$$d = \frac{c' + i_{on}\ r_{Ln}}{V_{ccn}} = \frac{c' + \Delta c}{V_{ccn}} \tag{3.33}$$

which combined with (3.15) leads to:

$$d_x = \frac{v_{Cn}(0)^2 + i_{Cn}(0)^2 - 1}{2\ V_{ccn}\ (v_{Cn}(0) - 1)} + \frac{i_{on}\ r_{Ln}}{V_{ccn}} \tag{3.34}$$

In this case, the duty cycle needed to lead the operating point to the target depends also on the load current and inductor normalized parasitic resistance.

The inductor series resistance varies in response to environmental parameters (eg: temperature); therefore a linear estimation is performed to approximate its value. The value of r_{Ln} changes in a very slow manner (order of seconds) which leads to very low dynamic requirements for the linear estimator.

The proposed controller is described by the block diagram of Fig. 3.15(a). Experimental results are shown in Fig. 3.15(b) and 3.16, validating the described behaviour. Since in this approach more information is required for the implementation of the controller, it has been excluded from the comparative analysis of section VI in order to perform a fair one-to-one comparison. Nevertheless, experimental results of this last approach for the same transients are presented in Fig. 3.16 (a) and (b) to illustrate the enhanced performance obtained. As expected, the voltage and current peak deviations during the transients show similar values to those in the previous centric-based case. The main differences are found in the neighborhood of the target operating point, where the small oscillations are avoided and the steady state is .reached merely by recalculating the center and setting the right duty cycle. It is also worthwhile noting that in this last case the duty cycle value changes by fewer larger steps, remaining steady most of the time. According to the requirements of the application, the extra variable needed to implement this version of the controller might be justified by the improvement in the dynamic response and the 100% predictable response obtained.

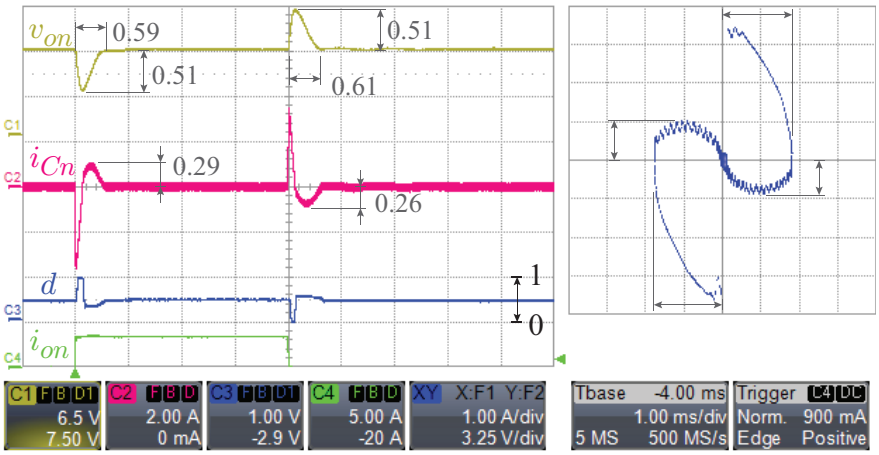

(a)

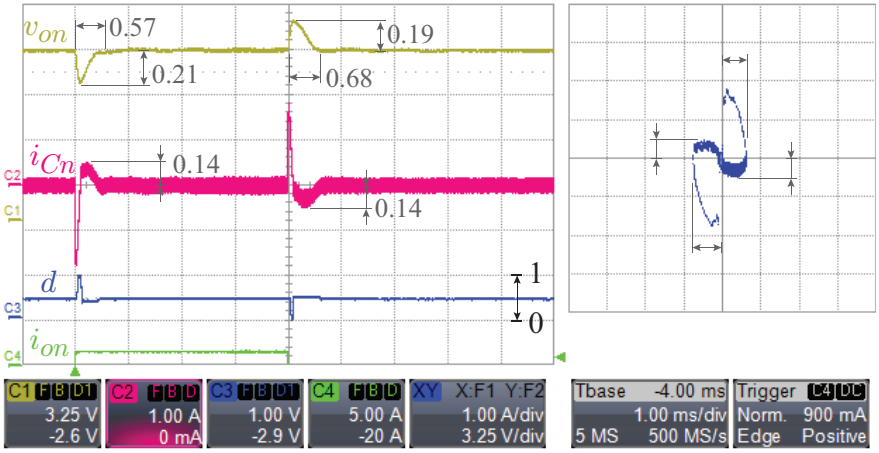

(b)

Figure 3.16: Response of the centric-based controller with load current measurement for loading/unloading transients with $\Delta i_{on} = 1$ (a), and $\Delta i_{on} = 0.5$(b).

3.9 Centric Controller Benchmark

In this section the centric-based controller is compared with the physical limits of performance derived in the previous chapter. In order to allow an objective assessment, the start-up, loading and unloading transient responses of the ideal centric-based controller are shown in Fig. 3.17, along with the physical limits of performance in both time and geometric domains.

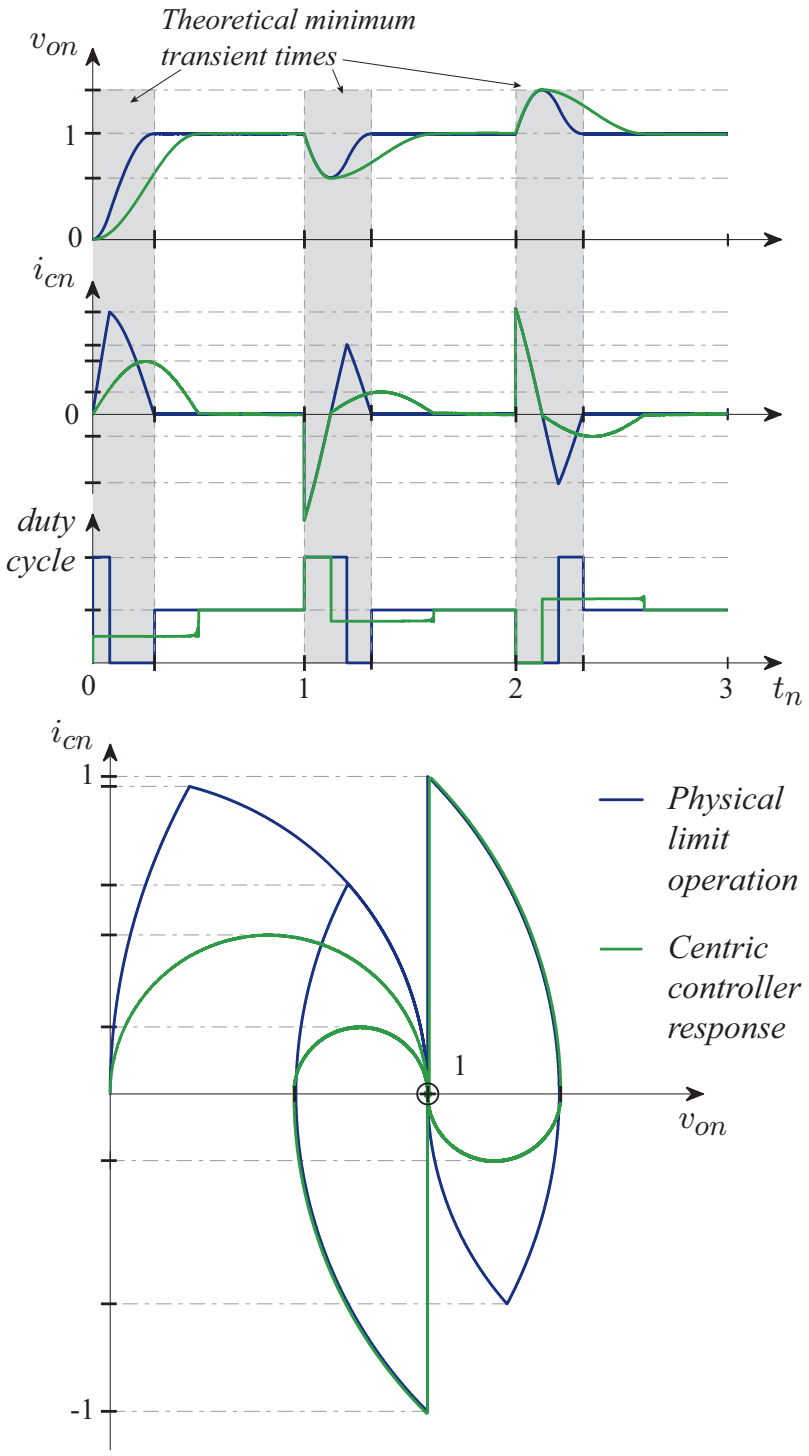

Figure 3.17: Performance comparison between the ideal centric-based controller and the dynamic physical limits.

As mentioned in the previous chapter, the ideal start-up transient only depends on the normalized input voltage and can take values from $T_0/4$ to $T_0/3$. In the case of the centric controller, the normalized settling time is constant. It is simple to observe that the start-up transient describes a half-circle for any input-output voltage ratio. Since the normalized angular speed is constant, the start-up is found to be:

$$t_{start-up}(centric) = \frac{\pi}{2\pi} = 0.5 \tag{3.35}$$

which, as expected, is always higher than the theoretical limit of performance. The start-up current peak of the novel technique is also constant, and presents a normalized value of 0.5.

Since the response shown in Fig. 3.17 corresponds to the ideal behaviour of the centric controller, and due to the duty cycle saturation algorithm implemented, the first portion of the loading/unloading transients coincide with the theoretical limits of performance. Once the capacitor current reaches zero, the transient response differs from the ideal and describes a half-circle, taking a time of $T_0/2$ to reach steady state. In this way, the theoretical voltage drops/peaks reached present values close to the ideal, while the recovery current peaks are maintained at lower values than in the ideal case.

3.10 Summary

This chapter presented the Averaged Natural Trajectories (ANTs) for buck converters, which were derived by using traditional averaging techniques on the converter state equations and representing them in the geometrical domain. Mathematical expressions to direct the operating point towards the target by performing calculations only at the initial instant were found and verified by experimental results.

A new type of geometric-based controller for buck converters, based on the large-signal model obtained in this chapter, was developed. The control laws to implement the novel

scheme were derived and validated by experimental results in a 44W prototype, showing fixed switching frequency and excellent transient performance.

The performance of centric-based and traditional dual-loop controllers was compared using experimental results corresponding to different transients. As a result of the comparison, the enhanced performance of the centric-based controller was verified by a faster recover, lower peak deviations in voltage and current, and a predictable evolution of the variables. The proposed control scheme was also tested under parameter deviations to ensure its reliable operation and suitability to be implemented in high volume applications. The controller performance was compared against the theoretical performance limits using the benchmark tool introduced in the previous chapter.

The work provides valuable conceptual and practical contributions to the field: the Average Natural Trajectories which accurately model the PWM driven converter large-signal behavior, and the high-performance control strategy that results from a centric-based PWM manipulation.

Chapter 4

Average Natural Trajectories (ANTs) for Boost Converters: Centric-Based Control

Two main novel concepts were introduced in the previous chapter for buck converters: the ANTs and the centric-based controller. The ideas are new in the field of controls for power electronics, and can be applied in any power conversion topology. In order to illustrate this fact, and due to the outstanding results obtained in buck converters, this chapter extends the theory and implementation to the basic boost DC-DC topology. A particular extra limitation is imposed by the characteristic non-minimum phase behavior of the boost topology, which gives traditional linear controllers a sluggish response. As in the previous case, the novel geometric-based controller is developed to combine the advantages of averaged and geometrical analysis. As a result, a fast and predictable dynamic performance is obtained while keeping fixed PWM frequencies and low-bandwidth sensing/sampling systems.

The natural response of the PWM driven boost converter is modeled by Averaged Natural Trajectories (ANTs), which are obtained by merging geometrical analysis and traditional average techniques. As a result of the normalized analysis, circular averaged trajectories valid for any combination of LC parameters are obtained as illustrated in Fig. 4.2. The insight provided by the obtained ANTs is used to develop a reliable fixed-frequency control scheme featuring fast and predictable dynamic performance and low bandwidth requirements

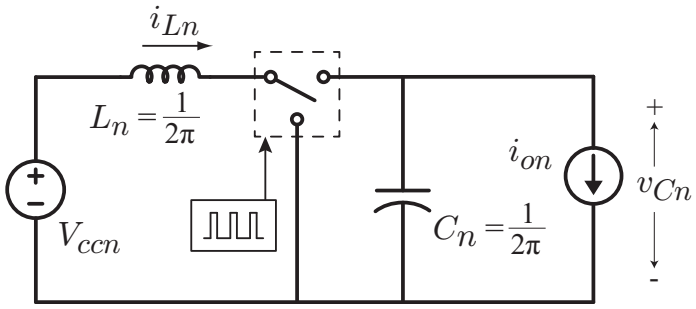

(a)

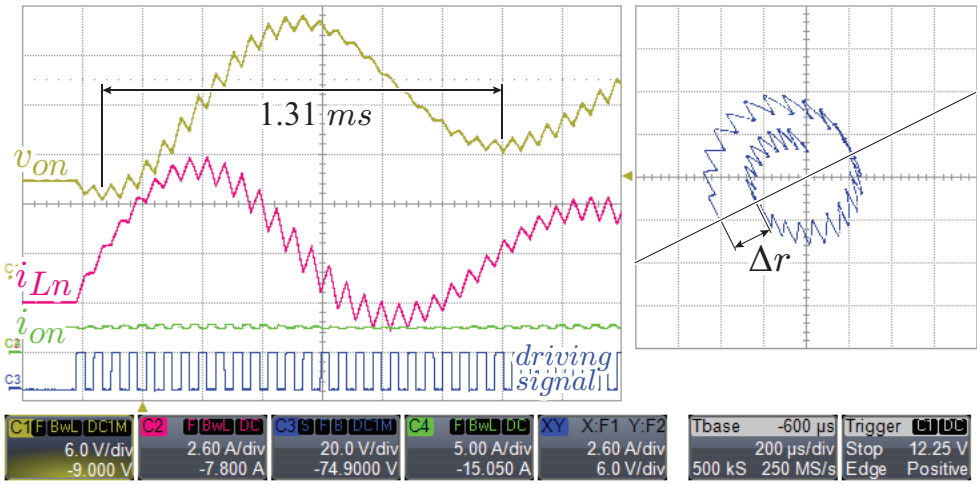

(b)

Figure 4.1: a) Normalized PWM driven boost converter. b) PWM natural trajectories in a real converter.

for sensing and signal conditioning stages. In contrast with boundary controllers where the control is performed by ON-OFF actions, in the centric-based controller it is done by setting a PWM duty cycle based on the current location and averaged behaviour of the converter. In the ideal case, the center is calculated only once in order to direct the operating point to the target, requiring a very low processing cost. The derivation of the control laws is presented along with the normalization procedure and the ANTs derivation for boost converters. Experimental results in open and closed loop validate the ANTs and the enhanced dynamic response of the centric controller, highlighting the strong contribution this work makes to both theoretical and applied fields.

4.1 Normalized Boost Converter ANTs Derivation

The Averaged Natural Trajectories of the ideal PWM driven normalized boost converter shown in Fig. 4.2 are developed in this section.

The differential equations that rule the behavior of boost converters are, for ON state:

$$C\frac{dv_C}{dt} = -i_o \tag{4.1}$$

$$L\frac{di_L}{dt} = V_{cc} \tag{4.2}$$

and for OFF state:

$$C\frac{dv_C}{dt} = i_L - i_o \tag{4.3}$$

$$L\frac{di_L}{dt} = V_{cc} - v_C \tag{4.4}$$

In order to gain generality, the analysis is taken to the normalized domain, where:

$$t_n = \frac{t}{T_0}; \qquad Z_{xn} = \frac{Z_x}{Z_0}; \qquad v_{xn} = \frac{v_x}{v_{ref}}; \qquad i_{xn} = \frac{i_x}{i_{ref}}$$

The base quantities employed are the filter characteristic impedance and resonance period, and the reference voltage and current:

$$Z_0 = \sqrt{L/C}; \qquad T_0 = 2\pi\sqrt{LC}; \qquad v_{ref}\ ; \qquad i_{ref} = \frac{v_{ref}}{Z_0}$$

As a result, the differential equations that describe the behaviour of the normalized boost converter are found for ON,

$$\frac{1}{2\pi}\frac{dv_{Cn}}{dt_n} = -i_{on} \tag{4.5}$$

$$\frac{1}{2\pi}\frac{di_{Ln}}{dt_n} = V_{ccn} \tag{4.6}$$

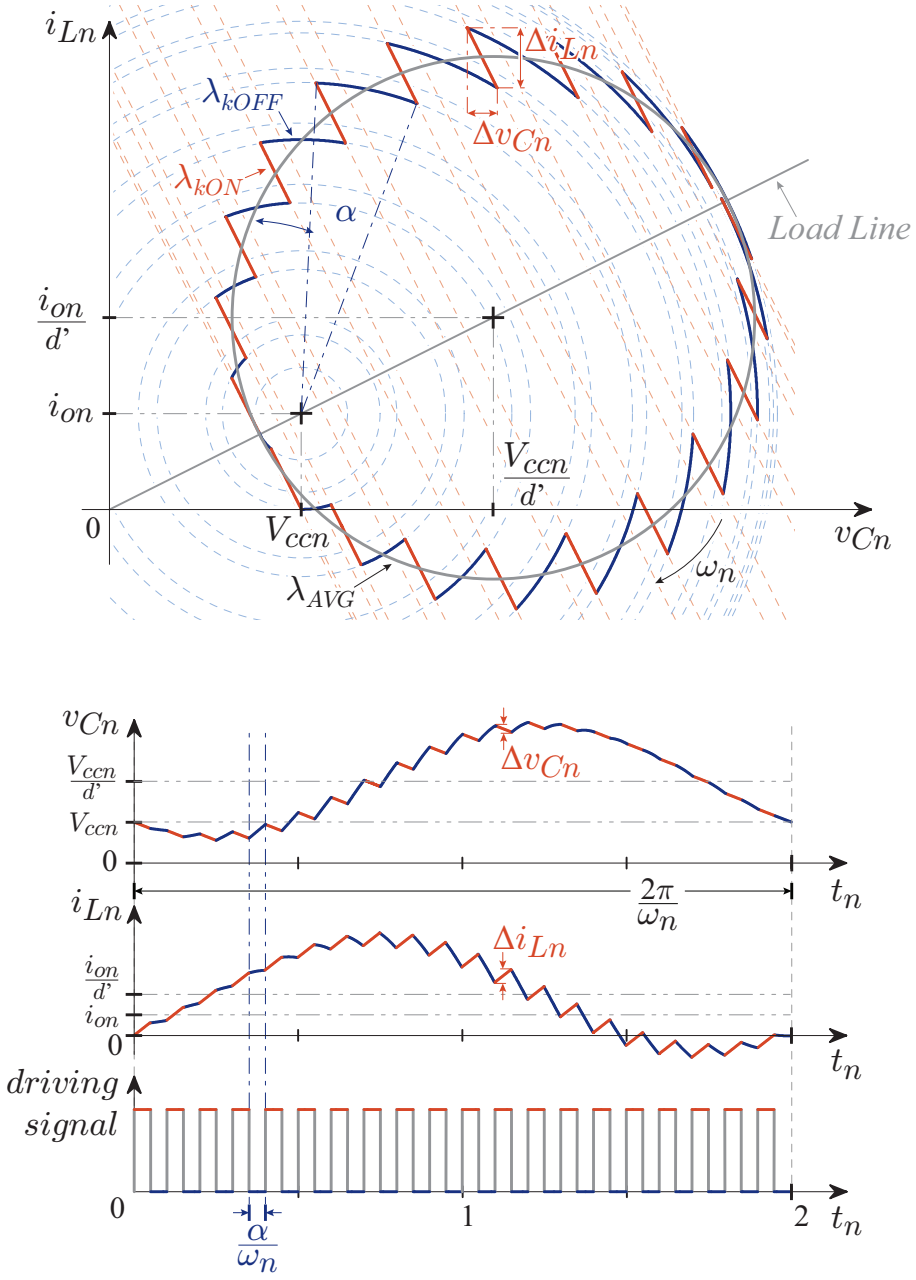

Figure 4.2: Ideal natural trajectories with $V_{ccn} = 0.5$, $d = 0.5$ and $f_{sn} = 10$.

and OFF states.

$$\frac{1}{2\pi}\frac{dv_{Cn}}{dt_n} = i_{Ln} - i_{on} \tag{4.7}$$

$$\frac{1}{2\pi}\frac{di_{Ln}}{dt_n} = V_{ccn} - v_{Cn} \tag{4.8}$$

Employing traditional averaging techniques [5], the averaged differential equations in normalized form are obtained:

$$\frac{1}{2\pi}\frac{dv_{Cn}}{dt_n} = d'\ i_{Ln} - i_{on} \tag{4.9}$$

$$\frac{1}{2\pi}\frac{di_{Ln}}{dt_n} = V_{ccn} - d'\ v_{Cn} \tag{4.10}$$

where: $d' = 1 - d$, is the complementary PWM duty cycle determined by the ratio between the OFF time (T_{OFF}) and the PWM period (T_s).

Time-domain expressions that describe the averaged evolution of the state variables (capacitor voltage and inductor current) can be found by solving the differential equations (4.9) and (4.10):

$$v_{Cn}(t_n) = [v_{Cn}(0) - \frac{V_{ccn}}{d'}]cos(d'\ 2\pi t_n) + [i_{Ln}(0) - \frac{i_{on}}{d'}]sin(d'\ 2\pi t_n) + \frac{V_{ccn}}{d'} \tag{4.11}$$

$$i_{Ln}(t_n) = [i_{Ln}(0) - \frac{i_{on}}{d'}]cos(d'\ 2\pi t_n) + [v_{Cn}(0) - \frac{V_{ccn}}{d'}]sin(d'\ 2\pi t_n) + \frac{i_{on}}{d'} \tag{4.12}$$

The expression that describes the Averaged Natural Trajectories (ANTs) that the operating point follows for the ideal PWM driven normalized boost converter is obtained by combining (4.11) and (4.12) and eliminating the normalized time variable t_n:

$$\lambda_{AVG} : \left[i_{Ln} - \frac{i_{on}}{d'}\right]^2 + \left[v_{on} - \frac{V_{ccn}}{d'}\right]^2 - \left[i_{Ln}(0) - \frac{i_{on}}{d'}\right]^2 - \left[v_{on}(0) - \frac{V_{ccn}}{d'}\right]^2 = 0 \tag{4.13}$$

The parametric equation obtained represents a circle with center located at $(\frac{V_{ccn}}{d'}; \frac{i_{on}}{d'})$, and radius determined by the initial conditions $[v_{Cn}(0); i_{Ln}(0)]$.

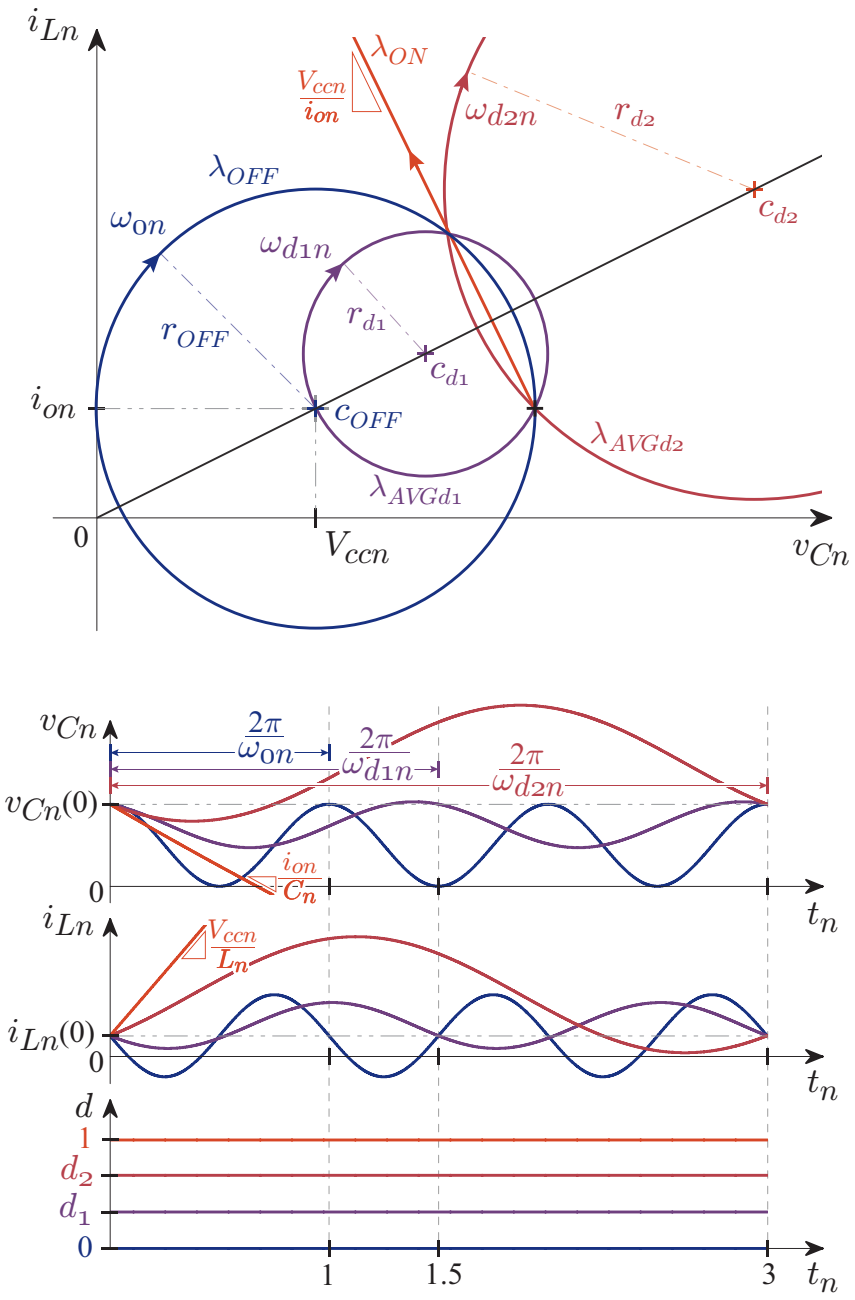

Figure 4.3: Several PWM-driven boost converter ANTs departing from unique initial operating point.

Several circular trajectories corresponding to the same initial conditions but different centers are shown in Fig. 4.3. It is worth noting that the center is always located on the load line, at a distance from the origin determined by the scalar $c = \frac{1}{d'}$ multiplied by the base vector $(V_{ccn}; i_{on})$.

Taking (4.11) and (4.12) into account, the normalized angular speed at which the operating point moves across the circular trajectory is found to be constant and defined by $\omega_n = d'\ 2\pi$, as illustrated by the time-domain plots in Fig. 4.3.

From a practical point of view, the natural resonance of the $L - C$ system is defined by the fraction of time the reactive components are connected together. For instance, when the system remains in OFF state, the inductance L and the capacitance C are connected all the time, which corresponds to the condition $d = 0$ and therefore $\omega_n = 2\pi$ ($\omega = \frac{1}{\sqrt{LC}}$), which represents the natural frequency of an LC resonant tank. It is also worth pointing out that when the system remains in ON state ($d = 1$), there is no interaction between the reactive components and therefore $\omega_n = 0$ and the circle becomes a straight line that is perpendicular to the load line as the center location tends towards infinity in the load line direction.

As indicated, the derived expressions are valid for the whole range of possible PWM duty cycles, including the saturation extremes $d = 0$ and $d = 1$. Therefore (4.13) represents a complete ideal averaged model of the normalized boost converter in the geometrical domain.

4.2 Approaching the Target

As determined in the previous section, for any given initial conditions the operating point follows an ANT determined by the PWM duty cycle. There is an ANT that leads the operating point to the target located at $(1; i_{Lnt})$, where the normalized target inductor current is: $i_{Lnt} = \frac{i_{on}}{V_{ccn}}$.

The center of the circle that contains both initial and target operating points can be

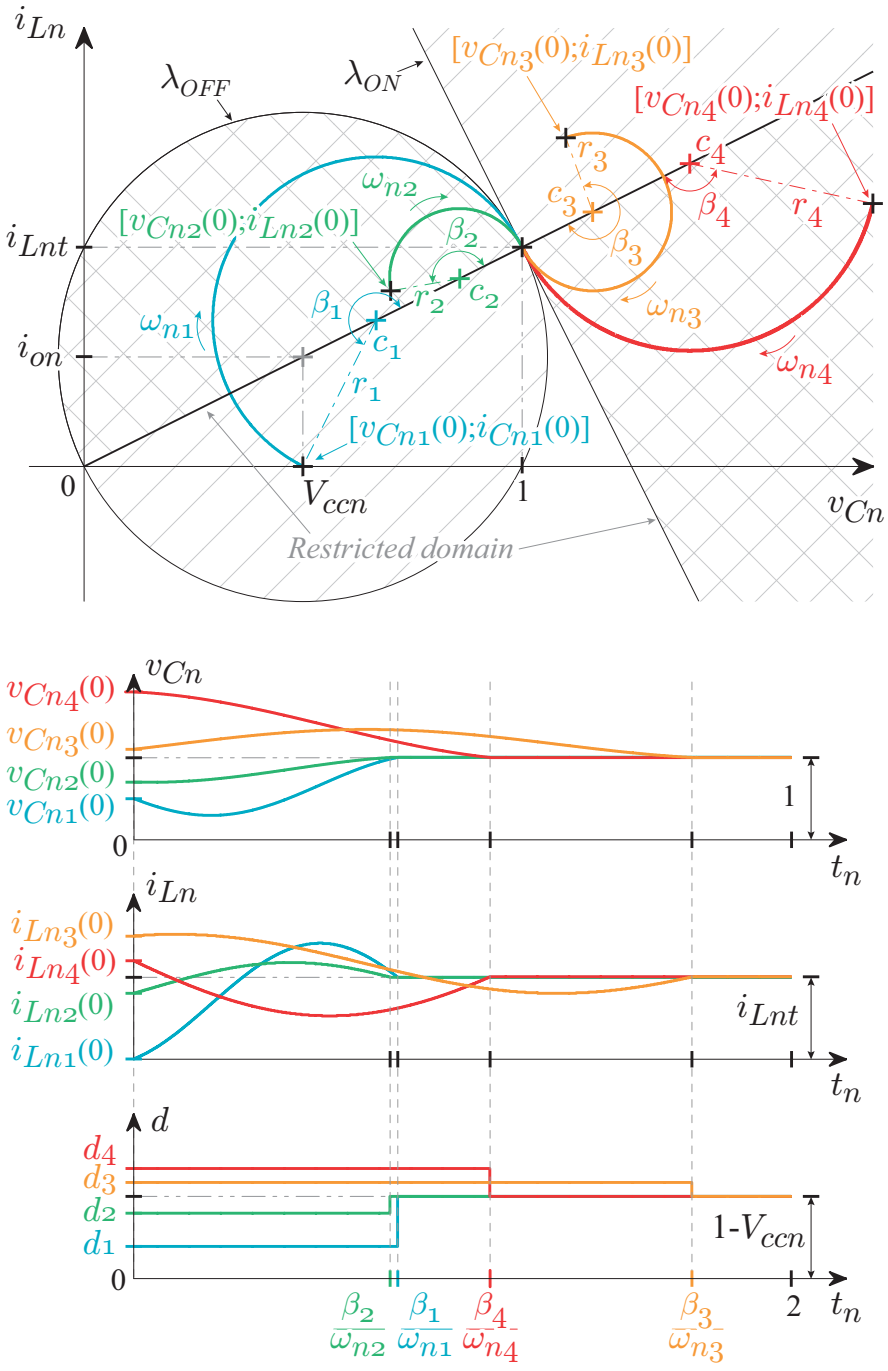

Figure 4.4: Fixed duty cycle target approaching method for different initial conditions

found by performing a geometrical analysis from Fig. 4.4:

$$c = 0.5\ \frac{v_{Cn}(0)^2 + i_{Ln}(0)^2 - i_{Lnt}^2 - 1}{V_{ccn}(v_{Cn}(0) - 1) + i_{on}(i_{Ln}(0) - i_{Lnt})} \tag{4.14}$$

Taking into account that $c = \frac{1}{1-d}$, the duty cycle to obtain the desired circle is found:

$$d = 1 - 2\ \frac{V_{ccn}(v_{Cn}(0) - 1) + i_{on}(i_{Ln}(0) - i_{Lnt})}{v_{Cn}(0)^2 + i_{Ln}(0)^2 - i_{Lnt}^2 - 1} \tag{4.15}$$

This expression is valid for any initial point located inside of the domain limited by the ON and OFF trajectories as indicated in Fig. 4.4, and determines the duty cycle needed to reach the target operating point following just one averaged circular path. The time the operating point takes to reach the target can be determined from Fig. 4.4 by finding the angle β_k and dividing it by $\omega_{kn} = d'\ 2\pi$:

$$t_D = \frac{1}{d'\ 2\pi}\ \left(tan^{-1}\left(\frac{i_{on}}{V_{ccn}}\right) - tan^{-1}\left(\frac{d'\ i_{Ln}(0) - i_{on}}{d'\ v_{cn}(0) - v_{cn}}\right)\right) \tag{4.16}$$

Once the target is reached, the center must be moved to the steady state operating point $(1; i_{Lnt})$ by setting the duty cycle to $1 - V_{ccn}$, in order to obtain an averaged circular trajectory with null radius. A simple and powerful principle is found: the desired steady state operating condition can be reached in a known time period and following a predictable circular trajectory. The only control action required to achieve this is to set the PWM duty cycle to a fixed value determined by the location of the initial and target operating points.

4.3 Closing the Loop with a Centric-Based Controller

Based on the target approaching method presented in the previous section, a novel fixed-frequency geometrical control scheme is proposed here. A periodical recalculation of the

center location using (4.15), allows the controller to compensate for deviations in the reactive components values, losses and any extra effect not being considered in the ANTs derivation that could move the trajectory beyond ideal circles. In this way, the distortion in the circular trajectories is limited to the value it reaches during one recalculation period.

As mentioned above, (4.15) is valid for any initial point located inside the ON and OFF natural trajectories. When the operating point is located outside of this domain, it is taken back in by saturating the duty cycle at its corresponding extreme. In order to improve the dynamic response, the function domain is restricted to the half of the λ_{OFF} circle located above the load line, and to the portion at the right of λ_{ON} below the load line as indicated in Fig. 4.4. In this way, the drops and peaks in the output voltage can be kept low during load transients, while large current spikes at the inductor are avoided, and a fast, predictable and reliable transient response is obtained.

A slow estimator of the series resistance is also implemented in order to account for series voltage drops. Even though in high efficiency converters the DC resistance in the inductor and switches are minimal, a small steady state error might be present but can be eliminated by using the load current and the series resistance estimation.

4.4 Experimental Results

The theoretical and applied concepts introduced in this chapter have been validated in the $65W$ boost converter detailed in Tables 4.1 and 4.2.

The Averaged Natural Trajectories are validated by experimental results in Fig. 4.1 (b), where the normalized switching frequency has been set to $f_{sn} = 10$ and the duty cycle to 50%. Observing the time-domain waveforms, the normalized resonance period of the system is found to be 2 (1.31 ms), as is to be expected for a $d' = 0.5$.

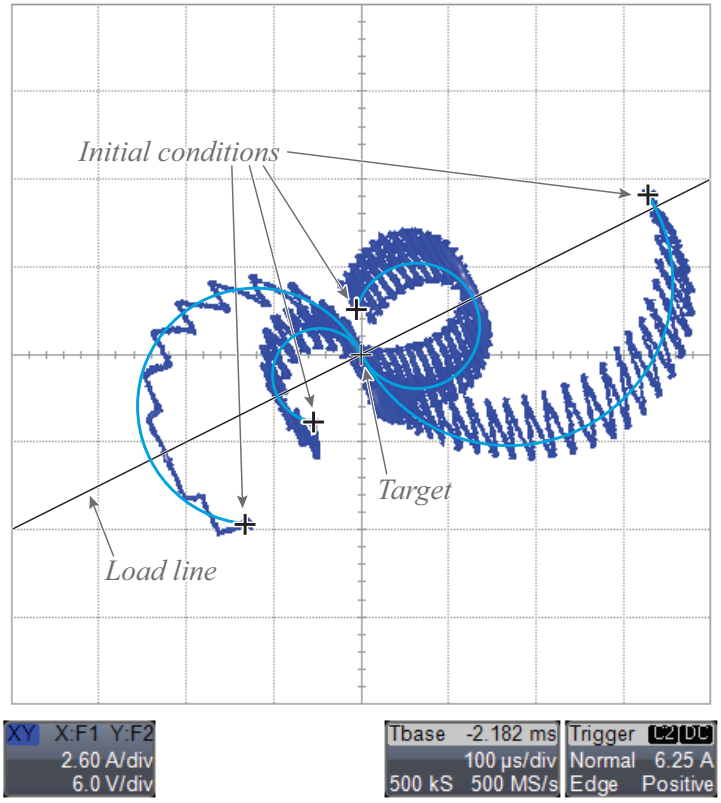

(a)

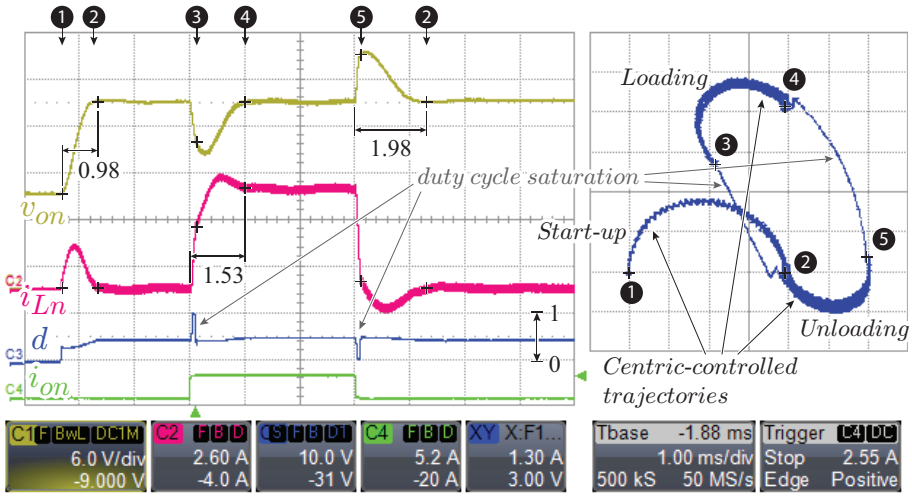

(b)

Figure 4.5: Centric-based controller experimental results. a) Open-loop with duty cycle precalculation. b) Closed-loop response for start-up, loading and unloading transients.

Table 4.1: Boost converter parameters

PARAMETER	VALUE	NORM.
v_{ref}	24 V	1
V_{cc}	12 V	0.5
L	240 μH	$\frac{1}{2\pi}$
C	45 μF	$\frac{1}{2\pi}$
T_0	654 μs	1
Z_0	2.3 Ω	1

Table 4.2: Main parasitics

PARAMETER	VALUE	NORM.
r_L	150 $m\Omega$	$65.2m$
r_C	43 $m\Omega$	$18.7m$
$r_{switch1}$	20 $m\Omega$	$6.15m$
$r_{switch2}$	20 $m\Omega$	$6.15m$

As shown in Fig. 4.1 (b), the real trajectories present differences from those derived for the ideal case; these differences are due to the effects of losses in the system.

Experimental results of the system working in open-loop with pre-calculated duty cycles that lead the operating point to the target for different initial conditions are shown in Fig. 4.5 (a), where $f_{sn} = 10$.

The enhanced dynamic performance of the closed-loop controller is validated by the fast and predictable recoveries from extremely large transients shown in Fig. 4.5 (b). Even though the normalized current step-up and step-down transients are extremely large, steady state is reached back in periods of time of the same order of magnitude (1.53 to 1.98) than the LC resonance period. Since the duty cycle saturation is implemented, the voltage drops and peaks are close to optimal, and due to the center placement technique, the inductor current peaks are kept low.

4.5 Summary

The Averaged Natural Trajectories (ANTs) for DC-DC boost converters were derived and presented in this chapter. The proposed large-signal model was developed combining traditional averaging techniques with a geometrical domain analysis of the normalized boost converter state variables.

A closed form expression to calculate the duty cycle necessary to direct the operating point towards the target following one circular ANT was found and verified by experimental results. A new type of closed-loop control technique for boost converters, featuring enhanced dynamic performance, fixed switching frequency and low bandwidth requirements, was developed and validated employing a 65 W prototype.

Chapter 5

Conclusions

5.1 Summary

This thesis introduced three novel concepts to the field of controls for power electronics: the physical limits of performance, the Average Natural Trajectories and the centric-based controller. The theoretical optimal response of the normalized buck converter to start-up, loading and unloading transients was found, analyzed and characterized by closed-form mathematical expressions. A powerful benchmark tool to analyze transient response in buck converters was introduced, and illustrated by an example of benchmarking procedure.

A novel model was developed for buck and boost converters by combining average, normalization and geometrical analysis. The Averaged Natural Trajectories provide valuable insight into the behaviour of power converters and accurately model the large-signal dynamics of the system. Due to the normalized approach, the models are valid for any combination of reactive components. The significant theoretical contribution to the field of modeling and controls must be highlighted.

Based on the model introduced in this work, a new type of geometric-based controller, suitable for high-volume applications, was developed for buck and boost converters. Due to the nature of the model employed, the controller features global stability, fixed switching frequency and an excellent dynamic performance. Furthermore, the control laws developed for both topologies can be implemented in converters with any combination of $L - C$ values, providing a universal solution and highly simplifying the design.

Performance comparisons with traditional linear techniques and a benchmark procedure using the physical limits of performance, were carried out for buck converters, confirming the enhanced dynamics and predictable behaviour of the proposed control scheme. The centric-based controlled buck converter was tested under deviations in the reactive components values in order to illustrate the robust characteristic of the proposed control technique.

The theoretical concepts introduced were supported by detailed mathematical procedures, and the control applications validated by simulation and experimental results.

The contribution of the work to the power conversion community is proven by the publication of [1–4]

5.2 Future Work

The concepts introduced in this work are original and were not known in the past, which highlights the importance of the contribution. A research paper about the physical limits of performance boost converters is being developed. A clear need to develop the theoretical optimal performance of other topologies and to work on the characterization of the controllers that are already on the field is identified.

The proposed large-signal model and control technique can be extended to other power converter topologies. These ideas are currently under development by the research team, being extended to other popular DC-DC topologies, as well as to active rectifiers and inverters.

Bibliography

[1] I. Galiano Zurbriggen, M. Ordonez, and M. Anun, "Dynamic physical limits of buck converters: The t0/4 transient benchmark rule," in *Applied Power Electronics Conference and Exposition (APEC), 2013 Twenty-Eighth Annual IEEE*, 2013, pp. 421–428. ©2013 IEEE.

[2] ——, "Average natural trajectories (ants) for buck converters: Centric-based control," in *Applied Power Electronics Conference and Exposition (APEC), 2013 Twenty-Eighth Annual IEEE*, 2013, pp. 1346–1351. ©2013 IEEE.

[3] ——, "Average natural trajectories (ants) for buck converters: Centric-based control," *Submitted to Power Electronics, IEEE Transactions on*, Aug. 2013.

[4] I. Galiano Zurbriggen and M. Ordonez, "Average natural trajectories (ants) for boost converters: Centric-based control," *Submitted to Applied Power Electronics Conference and Exposition (APEC), 2014 Twenty-Nine Annual IEEE*, Jul. 2013.

[5] G. Wester and R. Middlebrook, "Low-frequency characterization of switched dc-dc converters," *Aerospace and Electronic Systems, IEEE Transactions on*, vol. AES-9, no. 3, pp. 376–385, 1973.

[6] R. D. Middlebrook and S. Cuk, "A general unified approach to modeling switching-converter power stages," in *Proc. IEEE Power Electron. Spec. Conf. (PESC) 1976*, 1976, pp. 18–34.

[7] Y. Wen and O. Trescases, "Dc-dc converter with digital adaptive slope control in auxiliary phase for optimal transient response and improved efficiency," *Power Electronics, IEEE Transactions on*, vol. 27, no. 7, pp. 3396–3409, 2012.

[8] A. Babazadeh and D. Maksimovic, "Hybrid digital adaptive control for fast transient response in synchronous buck dc-dc converters," *Power Electronics, IEEE Transactions on*, vol. 24, no. 11, pp. 2625–2638, 2009.

[9] G. Feng, E. Meyer, and Y.-F. Liu, "A new digital control algorithm to achieve optimal dynamic performance in dc-to-dc converters," *Power Electronics, IEEE Transactions on*, vol. 22, no. 4, pp. 1489–1498, 2007.

[10] L. Yang, J. Park, and A. Huang, "An adaptive external ramp control of the peak current controlled buck converters for high control bandwidth and wide operation range," in *Applied Power Electronics Conference and Exposition (APEC), 2010 Twenty-Fifth Annual IEEE*, 2010, pp. 2181–2188.

[11] M. He and J. Xu, "Improved digital predictive control of switching dc-dc converters," in *Applied Power Electronics Conference, APEC 2007 - Twenty Second Annual IEEE*, 2007, pp. 1466–1471.

[12] A. Barrado, A. Roldan, J. Pleite, R. Vazquez, J. Vazquez, and E. Olias, "Linear-nonlinear control (lnlc) for dc-dc buck converters: stability and transient response analysis," in *Applied Power Electronics Conference and Exposition, 2004. APEC '04. Nineteenth Annual IEEE*, vol. 2, 2004, pp. 1329–1335 vol.2.

[13] L. Jia, Z. Hu, Y.-F. Liu, and P. Sen, "A practical control strategy to improve unloading transient response performance for buck converters," in *Energy Conversion Congress and Exposition (ECCE), 2011 IEEE*, 2011, pp. 397–404.

[14] L. Guo, J. Hung, and R. Nelms, "Digital controller design for buck and boost converters using root locus techniques," in *Industrial Electronics Society, 2003. IECON '03. The 29th Annual Conference of the IEEE*, vol. 2, 2003, pp. 1864–1869 Vol.2.

[15] O. Abdel-Rahman and I. Batarseh, "Transient response improvement in dc-dc converters using output capacitor current for faster transient detection," in *Power Electronics Specialists Conference, 2007. PESC 2007. IEEE*, 2007, pp. 157–160.

[16] S. Li, X. Zou, and X. Chen, "A nonlinear control buck converter with fast transient response," in *Integrated Circuits, ISIC '09. Proceedings of the 2009 12th International Symposium on*, 2009, pp. 45–48.

[17] L. Shi, M. Ferdowsi, and M. Crow, "Dynamic response improvement in a buck type converter using capacitor current feed-forward control," in *IECON 2010 - 36th Annual Conference on IEEE Industrial Electronics Society*, 2010, pp. 445–450.

[18] J.-P. Sjoroos, T. Suntio, J. Kyyra, and K. Kostov, "Dynamic performance of buck converter with input voltage feedforward control," in *Power Electronics and Applications, 2005 European Conference on*, 2005, pp. 9 pp.–P.9.

[19] A. Barrado, R. Vazquez, A. Roldan, J. Pleite, and E. Olias, "Fast transient response with combined linear-non-linear control applied to buck converters," in *Power Electronics Specialists Conference, 2002. pesc 02. 2002 IEEE 33rd Annual*, vol. 4, 2002, pp. 1587–1592.

[20] R. Singh and A. Khambadkone, "A buck-derived topology with improved step-down transient performance," *Power Electronics, IEEE Transactions on*, vol. 23, no. 6, pp. 2855–2866, 2008.

[21] A. Barrado, A. Lazaro, R. Vazquez, V. Salas, and E. Olias, "The fast response double

buck dc-dc converter (frdb): operation and output filter influence," *Power Electronics, IEEE Transactions on*, vol. 20, no. 6, pp. 1261–1270, 2005.

[22] X. Wang, I. Batarseh, S. Chickamenahalli, and E. Standford, "Vr transient improvement at high slew rate load mdash;active transient voltage compensator," *Power Electronics, IEEE Transactions on*, vol. 22, no. 4, pp. 1472–1479, 2007.

[23] S. Kapat, P. Shenoy, and P. Krein, "Near-null response to large-signal transients in an augmented buck converter: A geometric approach," *Power Electronics, IEEE Transactions on*, vol. 27, no. 7, pp. 3319–3329, 2012.

[24] E. Meyer, D. Wang, L. Jia, and Y.-F. Liu, "Digital charge balance controller with an auxiliary circuit for superior unloading transient performance of buck converters," in *Applied Power Electronics Conference and Exposition (APEC), 2010 Twenty-Fifth Annual IEEE*, 2010, pp. 124–131.

[25] K. Yao, Y. Meng, and F. Lee, "Control bandwidth and transient response of buck converters," in *Power Electronics Specialists Conference, 2002. pesc 02. 2002 IEEE 33rd Annual*, vol. 1, 2002, pp. 137–142 vol.1.

[26] M. Ordonez, J. Quaicoe, and M. Iqbal, "Critical parameters in the transient response of synchronous buck converters," in *Power Electronics Specialists Conference, 2007. PESC 2007. IEEE*, 2007, pp. 2189–2195.

[27] K. Yao, Y. Ren, and F. Lee, "Critical bandwidth for the load transient response of voltage regulator modules," *Power Electronics, IEEE Transactions on*, vol. 19, no. 6, pp. 1454–1461, 2004.

[28] R. Redl, B. Erisman, and Z. Zansky, "Optimizing the load transient response of the

buck converter," in *Applied Power Electronics Conference and Exposition, 1998. APEC '98. Conference Proceedings 1998., Thirteenth Annual*, vol. 1, 1998, pp. 170–176 vol.1.

[29] R. Muyshondt and P. Krein, "20 w benchmark converters for simulation and control comparisons," in *Computers in Power Electronics, 1998. 6th Workshop on*, 1998, pp. 201–212.

[30] A. Soto, A. De Castro, P. Alou, J. Cobos, J. Uceda, and A. Lotfi, "Analysis of the buck converter for scaling the supply voltage of digital circuits," *Power Electronics, IEEE Transactions on*, vol. 22, no. 6, pp. 2432–2443, 2007.

[31] G. Pitel and P. Krein, "Trajectory paths for dc - dc converters and limits to performance," in *Computers in Power Electronics, 2006. COMPEL '06. IEEE Workshops on*, 2006, pp. 40–47.

[32] ——, "Minimum-time transient recovery for dc-dc converters using raster control surfaces," *Power Electronics, IEEE Transactions on*, vol. 24, no. 12, pp. 2692–2703, 2009.

[33] M. Ordonez, M. Iqbal, and J. Quaicoe, "Selection of a curved switching surface for buck converters," *Power Electronics, IEEE Transactions on*, vol. 21, no. 4, pp. 1148–1153, 2006.

[34] S. Kapat and P. Krein, "Improved time optimal control of a buck converter based on capacitor current," *Power Electronics, IEEE Transactions on*, vol. 27, no. 3, pp. 1444–1454, 2012.

[35] M. Peretz and S. Ben-Yaakov, "Time-domain design of digital compensators for pwm dc-dc converters," *Power Electronics, IEEE Transactions on*, vol. 27, no. 1, pp. 284–293, 2012.

[36] M. Hallworth and S. Shirsavar, "Microcontroller-based peak current mode control using digital slope compensation," *Power Electronics, IEEE Transactions on*, vol. 27, no. 7, pp. 3340–3351, 2012.

[37] S. Kapat and P. Krein, "Formulation of pid control for dc-dc converters based on capacitor current: A geometric context," *Power Electronics, IEEE Transactions on*, vol. 27, no. 3, pp. 1424–1432, 2012.

[38] Y.-C. Lin, D. Chen, Y.-T. Wang, and W.-H. Chang, "A novel loop gain-adjusting application using lsb tuning for digitally controlled dc-dc power converters," *Industrial Electronics, IEEE Transactions on*, vol. 59, no. 2, pp. 904–911, 2012.

[39] Y.-S. Lai, Y.-T. Chang, and C.-T. Kuo, "Robust control of digital-controlled buck converter based upon two-degree-of-freedom controller," in *IECON 2010 - 36th Annual Conference on IEEE Industrial Electronics Society*, 2010, pp. 692–697.

[40] Y.-T. Chang and Y.-S. Lai, "Parameter tuning method for digital power converter with predictive current-mode control," *Power Electronics, IEEE Transactions on*, vol. 24, no. 12, pp. 2910–2919, 2009.

[41] S. Chattopadhyay and S. Das, "A digital current-mode control technique for dc-dc converters," *Power Electronics, IEEE Transactions on*, vol. 21, no. 6, pp. 1718–1726, 2006.

[42] A. Oliva, S. Ang, and G. Bortolotto, "Digital control of a voltage-mode synchronous buck converter," *Power Electronics, IEEE Transactions on*, vol. 21, no. 1, pp. 157–163, 2006.

[43] L. Jia and Y.-F. Liu, "Voltage-based charge balance controller suitable for both digital and analog implementations," *Power Electronics, IEEE Transactions on*, vol. 28, no. 2, pp. 930–944, 2013.

[44] E. Meyer, Z. Zhang, and Y.-F. Liu, "Digital charge balance controller to improve the loading/unloading transient response of buck converters," *Power Electronics, IEEE Transactions on*, vol. 27, no. 3, pp. 1314–1326, 2012.

[45] S. Huerta, P. Alou, O. Garcia, J. Oliver, R. Prieto, and J. Cobos, "Hysteretic mixed-signal controller for high-frequency dc-dc converters operating at constant switching frequency," *Power Electronics, IEEE Transactions on*, vol. 27, no. 6, pp. 2690–2696, 2012.

[46] P. T. Krein, *Nonlinear phenomena in power electronics: Attractors, bifurcation, chaos, and nonlinear control.* Piscataway, NJ: IEEE Press, 2001, ch. 8.

[47] M. Greuel, R. Muyshondt, and P. Krein, "Design approaches to boundary controllers," in *Power Electronics Specialists Conference, 1997. PESC '97 Record., 28th Annual IEEE*, vol. 1, 1997, pp. 672–678 vol.1.

[48] S.-C. Tan, Y. Lai, and C. Tse, "General design issues of sliding-mode controllers in dc-dc converters," *Industrial Electronics, IEEE Transactions on*, vol. 55, no. 3, pp. 1160–1174, 2008.

[49] R. Munzert and P. Krein, "Issues in boundary control [of power convertors]," in *Power Electronics Specialists Conference, 1996. PESC '96 Record., 27th Annual IEEE*, vol. 1, 1996, pp. 810–816 vol.1.

[50] P. Krein and R. Bass, "Types of instability encountered in simple power electronic circuits: unboundedness, chattering, and chaos," in *Applied Power Electronics Conference and Exposition, 1990. APEC '90, Conference Proceedings 1990., Fifth Annual*, 1990, pp. 191–194.

[51] B. Labbe, B. Allard, X. Lin-Shi, and D. Chesneau, "An integrated sliding-mode buck

converter with switching frequency control for battery-powered applications," *Power Electronics, IEEE Transactions on*, vol. 28, no. 9, pp. 4318–4326, 2013.

[52] W.-T. Yan, K. Au, C.-m. Ho, and H.-H. Chung, "Fixed-frequency boundary control of buck converter with second-order switching surface," *Power Electronics, IEEE Transactions on*, vol. 24, no. 9, pp. 2193–2201, 2009.

[53] S.-C. Tan, Y. Lai, M. Cheung, and C. Tse, "On the practical design of a sliding mode voltage controlled buck converter," *Power Electronics, IEEE Transactions on*, vol. 20, no. 2, pp. 425–437, 2005.

[54] R. Ramos, D. Biel, E. Fossas, and F. Guinjoan, "A fixed-frequency quasi-sliding control algorithm: application to power inverters design by means of fpga implementation," *Power Electronics, IEEE Transactions on*, vol. 18, no. 1, pp. 344–355, 2003.

[55] B. Cardoso, A. Moreira, B. Menezes, and P. Cortizo, "Analysis of switching frequency reduction methods applied to sliding mode controlled dc-dc converters," in *Applied Power Electronics Conference and Exposition, 1992. APEC '92. Conference Proceedings 1992., Seventh Annual*, 1992, pp. 403–410.

[56] M. Ordonez, J. Quaicoe, and M. Iqbal, "Advanced boundary control of inverters using the natural switching surface: Normalized geometrical derivation," *Power Electronics, IEEE Transactions on*, vol. 23, no. 6, pp. 2915–2930, 2008.

[57] W. Burns and T. Wilson, "A state-trajectory control law for dc-to-dc converters," *Aerospace and Electronic Systems, IEEE Transactions on*, vol. AES-14, no. 1, pp. 2–20, 1978.

[58] ——, "State trajectories used to observe and control dc-to-dc converters," *Aerospace and Electronic Systems, IEEE Transactions on*, vol. AES-12, no. 6, pp. 706–717, 1976.

[59] K. Kittipeerachon and C. Bunlaksananusorn, "Feedback compensation design for switched mode power supplies with a right-half plane (rhp) zero," in *Power Electronics, Machines and Drives, 2004. (PEMD 2004). Second International Conference on (Conf. Publ. No. 498)*, vol. 1, 2004, pp. 236–241 Vol.1.

[60] N. Kondrath and M. Kazimierczuk, "Control-to-output transfer function of peak current-mode controlled pwm dc-dc boost converter in ccm," *Electronics Letters*, vol. 47, no. 17, pp. 991–993, 2011.

[61] J. Sun and R. M. Bass, "Modeling and practical design issues for average current control," in *Applied Power Electronics Conference and Exposition, 1999. APEC '99. Fourteenth Annual*, vol. 2, 1999, pp. 980–986 vol.2.

[62] A. Urtasun, P. Sanchis, and L. Marroyo, "Adaptive voltage control of the dc/dc boost stage in pv converters with small input capacitor," *Power Electronics, IEEE Transactions on*, vol. 28, no. 11, pp. 5038–5048, 2013.

[63] S. El Beid and S. Doubabi, "Dsp-based implementation of fuzzy output tracking control for a boost converter," *Industrial Electronics, IEEE Transactions on*, vol. 61, no. 1, pp. 196–209, 2014.

[64] Z. Shen, N. Yan, and H. Min, "A multimode digitally controlled boost converter with pid autotuning and constant frequency/constant off-time hybrid pwm control," *Power Electronics, IEEE Transactions on*, vol. 26, no. 9, pp. 2588–2598, 2011.

[65] K. Mehran, D. Giaouris, and B. Zahawi, "Stability analysis and control of nonlinear phenomena in boost converters using model-based takagi-sugeno fuzzy approach," *Circuits and Systems I: Regular Papers, IEEE Transactions on*, vol. 57, no. 1, pp. 200–212, 2010.

[66] J. Neely, S. Pekarek, and R. DeCarlo, "Hybrid optimal-based control of a boost converter," in *Applied Power Electronics Conference and Exposition, 2009. APEC 2009. Twenty-Fourth Annual IEEE*, 2009, pp. 1129–1137.

[67] K. I. Hwu and Y. Yau, "Performance enhancement of boost converter based on linear-to-nonlinear translator," in *Applied Power Electronics Conference and Exposition, 2009. APEC 2009. Twenty-Fourth Annual IEEE*, 2009, pp. 1344–1347.

[68] S. Hiti and D. Borojevic, "Robust nonlinear control for boost converter," *Power Electronics, IEEE Transactions on*, vol. 10, no. 6, pp. 651–658, 1995.

[69] L. Martinez-Salamero, G. Garcia, M. Orellana, C. Lahore, and B. Estibals, "Start-up control and voltage regulation in a boost converter under sliding-mode operation," *Industrial Electronics, IEEE Transactions on*, vol. 60, no. 10, pp. 4637–4649, 2013.

[70] Y. He and F. Luo, "Sliding-mode control for dc-dc converters with constant switching frequency," *Control Theory and Applications, IEE Proceedings* -, vol. 153, no. 1, pp. 37–45, 2006.

[71] H. Wang, H. Chung, and J. Presse, "A unified derivation of second-order switching surface for boundary control of dc-dc converters," in *Energy Conversion Congress and Exposition, 2009. ECCE 2009. IEEE*, 2009, pp. 2889–2896.

[72] J. Galvez, M. Ordonez, T. Nguyen, and F. Luchino, "Boundary control of buck-boost converters: normalized trajectories and the natural switching surface," in *Energy Conversion Congress and Exposition (ECCE), 2012 IEEE*, 2012, pp. 358–363.

[73] J. Galvez, M. Ordonez, F. Luchino, and J. Quaicoe, "Improvements in boundary control of boost converters using the natural switching surface," *Power Electronics, IEEE Transactions on*, vol. 26, no. 11, pp. 3367–3376, 2011.